CHAPTER 4

PHOTOCATALYTIC DEGRADATION OF ORGANIC POLLUTANTS BY USING ZnFe LAYERED DOUBLE HYDROXIDE (LDH)

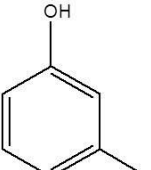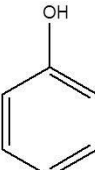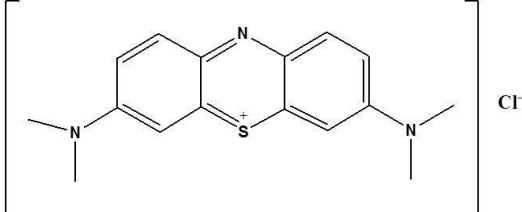This chapter describes complete characterization of ZnFe LDH synthesized via simple co-precipitation method. The activity measurements of the synthesized LDH towards the photocatalytic degradation of various organic pollutants have been discussed herein. The synthetic procedure of ZnFe LDH and characterization techniques are described in Chapter 2. Various organic pollutants used in the present investigation are listed in Table 4.1.

Table 4.1. The list of various organic pollutants used in the present investigation.

Organic pollutants	Chemical structures
Phenol	
2-Chlorophenol (2CP)	
3-Chlorophenol (3CP)	
4-Chlorophenol (4CP)	
Methylene blue (MB)	

Rhodamine B (RhB)
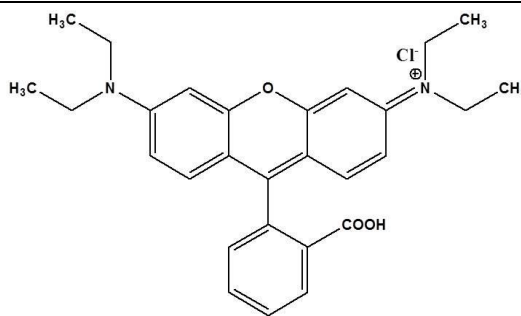
4.1 Prologue

Phenolic compounds have their extensive usages in various chemicals, petrochemicals, refineries and pharmaceuticals industries [1–3]. Phenols are also used as raw materials in the manufacture of various important organic compounds [4]. However, these compounds are very toxic, considered as a serious group of pollutants and they significantly contribute to water pollution. Elimination of these toxic compounds in the form of industrial effluents and other artificial activities cause severe environmental pollution. Phenol and their compounds produce unpleasant taste and odor, when come in contact with drinking water [5–8]. Moreover, these compounds are stable, non-degradable and have mutagenic and carcinogenic potential; and thus adversely effect on human health and aquatic life [9–12]. Therefore, treatment of these toxic compounds before it being released into the environment becomes a major and serious issue.

Moreover, the use of organic dyes in paper, textile, cosmetics, leather and food industries is well known [13–15]. The effluents released from these industries contain large quantity of dyes and therefore, in contact with water bodies cause serious water pollution [13]. Dyes in water bodies reduce visibility and light penetration and also increase the chemical oxygen demand (COD) [16,17]. Because of their stable, toxic and carcinogenic properties, dyes can significantly threaten to aquatic life and human health and thus they are considered as potentially dangerous [18,19]. Therefore, due to the increasing environmental risk, treatment of the dye contaminants is needed before being discharged into the environment.

It is vital to adopt an efficient technique for the treatment of such organic contaminants by transforming them into less toxic mineralized products. Heterogeneous photocatalysis is considered as an emerging technique with the advantages of low-cost, environmental friendly for the efficient removal of phenolic compounds from aqueous solution. Photocatalysis is a type of advanced oxidation process (AOP) in which highly active oxidative species such as $^\cdot$OH or H_2O_2 are generated in presence of light irradiation, which facilitate the degradation process in aqueous medium leading to the mineralization of organic pollutants to harmless products as H_2O, CO_2 and smaller ions such as Cl^-, SO_4^{2-} etc. [20–23]. Titanium dioxide, TiO_2 is considered as the most efficient semiconductor photocatalysts due to its high efficiency, less toxicity and low cost [24]. However, the fast electron−hole pair recombination, wide band gap ($E_g > 3.20$ eV) and difficulty in separation of the powdered catalyst from the suspension limits their practical use [25–27]. Therefore, it is necessary to develop such a photocatalyst with optimal band gap that enhance the photoactivity for environmental remediation by inhibiting the electron−hole pair recombination and also can be regenerated for reuse.

Recently, layered double hydroxides (LDHs) as photocatalyst have drawn increasing attention towards the treatment of organic contaminants [28,29]. The unique properties of LDHs such as high surface area, high adsorption capacity, thermal stability, easily tailored properties with versatile compositions, adjustable surface basicity, exchangeable interlayer anions, memory effect etc. [30,31] make it highly demandable research area for the scientist all over the globe [32]. The presence of surface –OH group in the LDH structure make it an interesting material of choice as photocatalyst for the oxidative degradation of organic pollutants.

4.2 Results and discussion

4.2.1 Characterization of ZnFe LDH

The formation of hydrotalcite-like LDH and their crystalline nature can be depicted from the XRD pattern of ZnFe LDH (Figure 4.1). The XRD pattern exhibits characteristic diffraction peaks of typical well crystallized LDH material. Sharp and highly intense diffraction peaks are observed at lower side of $2\theta = 11.6$, 23.4 and 34.7° corresponding to

the (003), (006) and (009) reflection planes, respectively. The broad, less intense peaks are observed at higher side of 2θ angles i.e. at $2\theta = 39.0$, 46.1, 60.7 and 62.1° corresponding to (015), (012), (110) and (113) reflection planes, respectively.
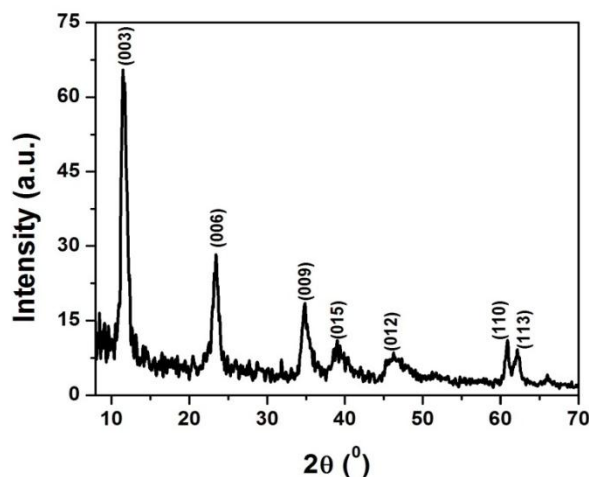

Figure 4.1. Powder XRD patterns of ZnFe LDH.

Various lattice parameters of the sample have been calculated and presented in Table 4.2. The lattice parameter 'c' is related with the interlayer spacing and thickness of the brucite layers whose value depends upon the charge of metal cation, size and charge of the interlayer anions and also on the water contents. The lattice parameter 'a' is the average metal ion distances within the brucite layers. The calculated d-spacing of ZnFe LDH is 7.69 Å which is almost closer to the literature [33].

Table 4.2. Lattice parameters, crystallite size, band gap energy, BET surface area, pore volume and pore diameter of ZnFe LDH.

Catalyst	Lattice parameters (Å)			Crystallite size (Å)	Band gap (eV)	BET surface area (m²/g)	Pore volume (cm³/g)	Pore diameter (Å)
	d_{003}	c	a					
ZnFe LDH	7.69	23.08	3.05	84.1	2.18	90.7	16.1	3.22

The average crystallite size (D) of ZnFe LDH is determined by using equation 2.1. The calculated value of crystallite size further confirms the crystalline nature of the LDH sample (84.1 Å, Table 4.2).

Figure 4.2 shows the FTIR spectrum of ZnFe LDH. The absorption bands associated with the O–H stretching vibrations of surface hydroxyl group and interlayer water molecules is observed at around 3525 cm^{-1}. The band corresponding to the O–H bending vibration of water molecule is observed at 1647 cm^{-1}. The appearance of sharp and intense absorption band at nearly 1380 cm^{-1} is corresponding to the vibrations of CO_3^{2-} ions in the interlayer region. The band observed in the low frequency regions (bands below 1000 cm^{-1}) are corresponding to M–OH and M–O–M vibrations of the brucite layers. Thus, the formation of hydrotalcite-like LDH is well supported by the formation of characteristic absorption bands.
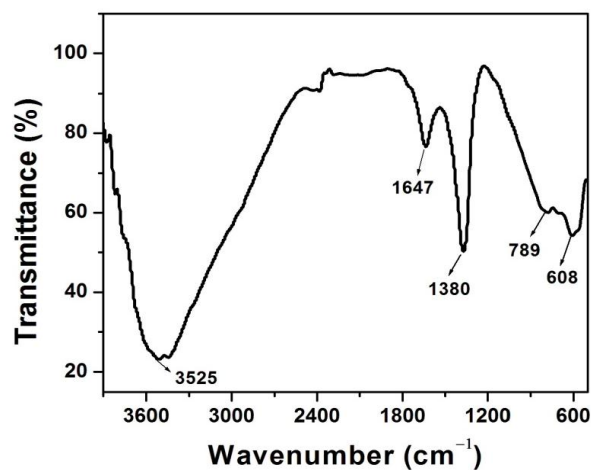

Figure 4.2. FTIR spectrum of ZnFe LDH.

The thermal stability of the LDH material has been carried out by thermogravimetric analysis and displayed in Figure 4.3. The TGA thermogram exhibits mainly two weight losses at two different temperatures. The weight loss at temperature around 50–100 °C is associated with the loss of surface water molecules. The second weight loss is associated with the decarboxylation of the carbonate anions as well as the dehydroxylation of water molecules present in the interlayer region of brucite-like LDH, observed in the temperature ranges of 250–500 °C.
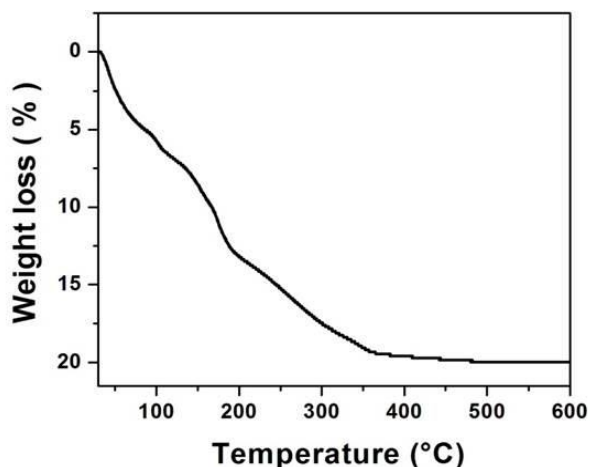
Figure 4.3. TGA thermogram of ZnFe LDH.

To understand the surface morphology of the LDH sample, SEM and TEM analysis have been performed. Figure 4.4 (a,b) shows the SEM images of ZnFe LDH at different magnifications with spongy like morphology resulting from the particles lying one above another. These aspects are further confirmed from the TEM image shown in Figure 4.4c. The crystallites possessing flat plate like morphology are lying on top of each other resulting in the irregular particle size. Figure 4.4d shows the corresponding selected area electron diffraction (SAED) pattern of the LDH. The formation of the concentric rings can visualized from the bright dots which correspond to the presence of different crystal planes. Thus, these findings suggest the uniform and crystalline nature of the LDH.

The light absorption behavior of the LDH has been determined by UV-visible diffuse reflectance spectroscopy and the result is displayed in Figure 4.5a. The adsorption band in the UV range (200–300 nm), which is exclusively due to the LMCT (ligand to metal charge transfer) transitions in the brucite-like layered structure. The optical absorbance is further extended to the photo active visible ranges of 500–800 nm owing to the MMCT (metal to metal charge transfer) transitions of oxo bridge bimetallic linkage (M^{II}–O–M^{III}).
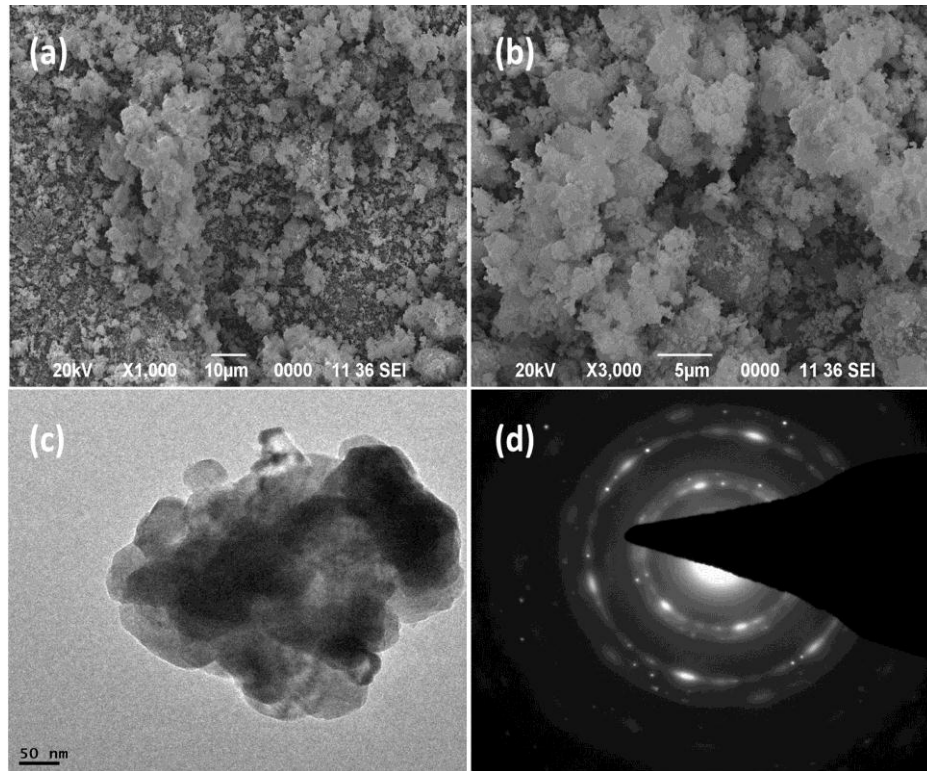
Figure 4.4. SEM images at (a) lower and (b) higher resolutions, (c) TEM image and (d) SAED patterns of ZnFe LDH.
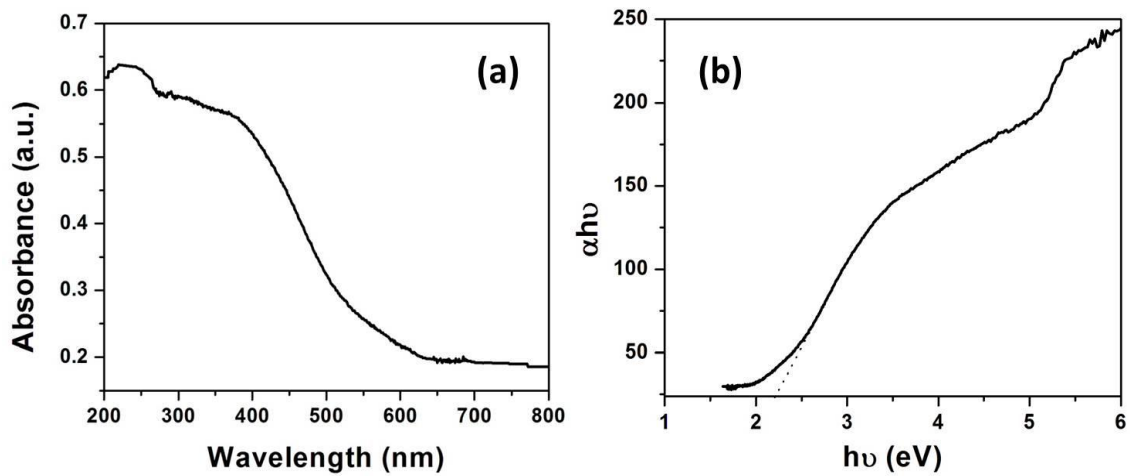

Figure 4.5. (a) UV-vis diffuse reflectance spectra and (b) corresponding band gap energy of ZnFe LDH.

The optical band gap energy (E_g) of the LDH has been determined by the Tauc/Davis–Mott expression as,

$$(\alpha h\upsilon)^{1/n_t} = A\left(h\upsilon - E_g\right) \qquad\qquad (4.1)$$

where, $h\upsilon$ is the energy of photon; α and A denotes the absorption coefficient and constant of proportionality, respectively. The 'n_t' value determines the characteristics of the transition in a semiconductor [34]. If the value of $n_t = 1$, it is a direct transitions and when the value of $n_t = 4$, the transition is an indirect transition. Here, the n_t value is found to be 1 which indicates that the transitions are directly allowed. The extrapolation of the curve to the x–axis has done to calculate the band gap energy (E_g) (Figure 4.5b) and the value obtained is 2.18 eV (Table 4.2).

The N_2 adsorption desorption measurement of ZnFe LDH has been carried out to explore the surface properties of the material. Figure 4.6a shows the N_2 adsorption desorption isotherm of the LDH material. The material exhibits the characteristics of a mesoporous material with formation of adsorption desorption isotherm of type IV [35]. The isotherm also exhibits the hysteresis loop of H2 type (type E as termed formerly) typical of mesoporous with regular narrow pore size distribution correlated with the aggregation of particles with plate-like morphology [33,36].The upper closer point of the hysteresis loop is appeared at higher value of relative pressure signifying porous nature of the material with large, open pores. Thus, it makes easier for the reactant molecules to diffuse through the material. Figure 4.6b shows the pore size distribution (PSD) curve of the LDH material. The curve is quite broad and bimodal with the appearance of small pores at 6.15 and 14.2 nm; and larger pore at 37.9 nm. The appearance of small and larger mesopores is associated with the pores within the LDH sheets and between the stacked sheets, respectively. The calculated specific surface area and pore volume of the LDH material are 90.7 m^2/g and 1.84 cm^3/g, respectively with average pore diameter (calculated from the desorption branch of the isotherm) of 3.22 nm. All the values of BET surface area, pore volume and pore diameter of the LDH material are presented in Table 4.2.
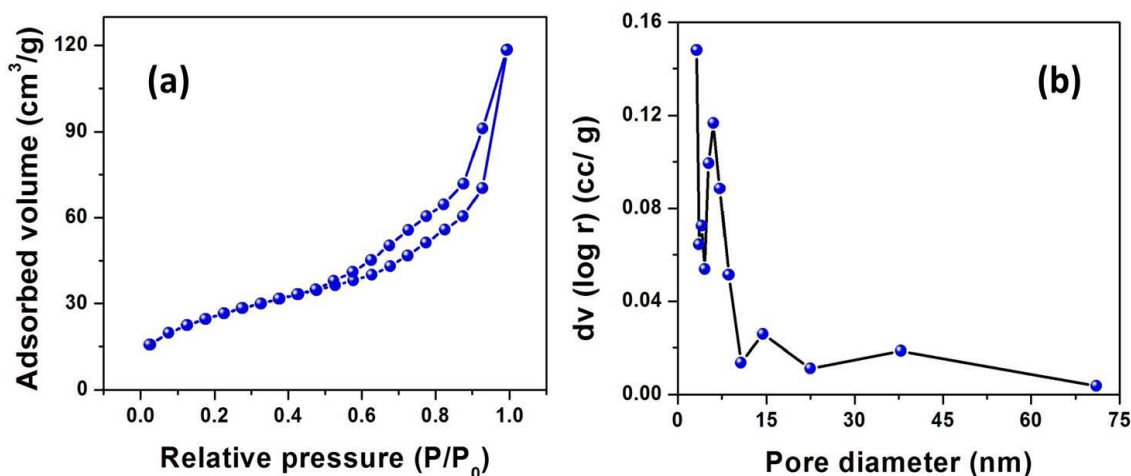
Figure 4.6. (a) N_2 adsorption-desorption isotherms, and (b) pore size distribution (PSD) curve of ZnFe LDH.

4.2.2   Catalytic activity of ZnFe LDH

ZnFe LDH has been employed for photocatalytic degradation of various phenolic compounds and organic dye pollutants in aqueous solution. Hence, the imminent part of this chapter is divided into two sections.

Section 4A: Photocatalytic degradation of phenol and its derivatives using ZnFe Layered Double Hydroxide (LDH)

This section briefly describes the catalytic activity of ZnFe LDH for oxidative degradation of phenol and its various compounds in aqueous solution under both visible and UV light irradiations. The detailed procedure of photocatalytic reactions have been described in Chapter 2.

4A.1   Photocatalytic degradation of phenol and its compounds

The photocatalytic activity of the prepared ZnFe LDH was first employed for degradation of phenol under different light irradiations. Prior to expose under light irradiation, adsorption study of phenol solution was employed over the catalyst in dark for 30 min in order to achieve an adsorption-desorption equilibrium. It has been observed that very small or negligible amount of phenol get adsorbed over the catalyst surface. After that, the

phenol solution was immediately exposed to light irradiation for photodegradation. The experiment was first carried out under visible light irradiation and degradation of phenol has measured from the corresponding UV-visible spectra (Figure 4A.1a). The catalyst shows excellent catalytic activity towards the photodegradation of phenol under visible light irradiation with 100% degradation in 120 min. It is observed that the maximum absorbance peak of phenol (λ_{max} = 270 nm) gradually decreases with irradiation time on exposure to the visible light irradiation and diminishes completely after the reaction. The appearance of various peaks at 276 and 289 nm suggest that the phenol degradation proceeds through various transient states such as catechol and hydroquinone, respectively. However, the transient p-benzoquinone (249 nm) was not detected clearly in the UV-vis spectra, which can be ascribed to the fast reaction. The aromatic ring opening of phenol takes place resulting subsequent formation of various aliphatic acids; and finally mineralized products such as carbon dioxide and water. For comparison, the photocatalytic experiments were also subjected under UV light irradiation and the corresponding UV-visible spectra is shown in Figure 4A.1b. Complete degradation of phenol was also observed under UV light irradiation, but, only when the irradiation time was increased upto 300 min. Figure 4A.1c shows the photodegradation of phenol as a function of time under different light irradiations. It is clearly seen that the concentration of phenol decreases faster with time on exposed under visible light irradiation compared to UV light and reaches almost zero in 120 min. The activity of the photocatalyst was further extended to various other phenolic compounds such as 2-chlorophenol (2CP), 3-chlorophenol (3CP) and 4-chlorophenol (4CP) under similar experimental conditions. Adsorption study was also carried out for 2CP, 3CP and 4CP in dark for 30 min prior to expose under light. Figure 4A.1d shows the photodegradation of various phenolic compounds with irradiation time under visible light irradiation.
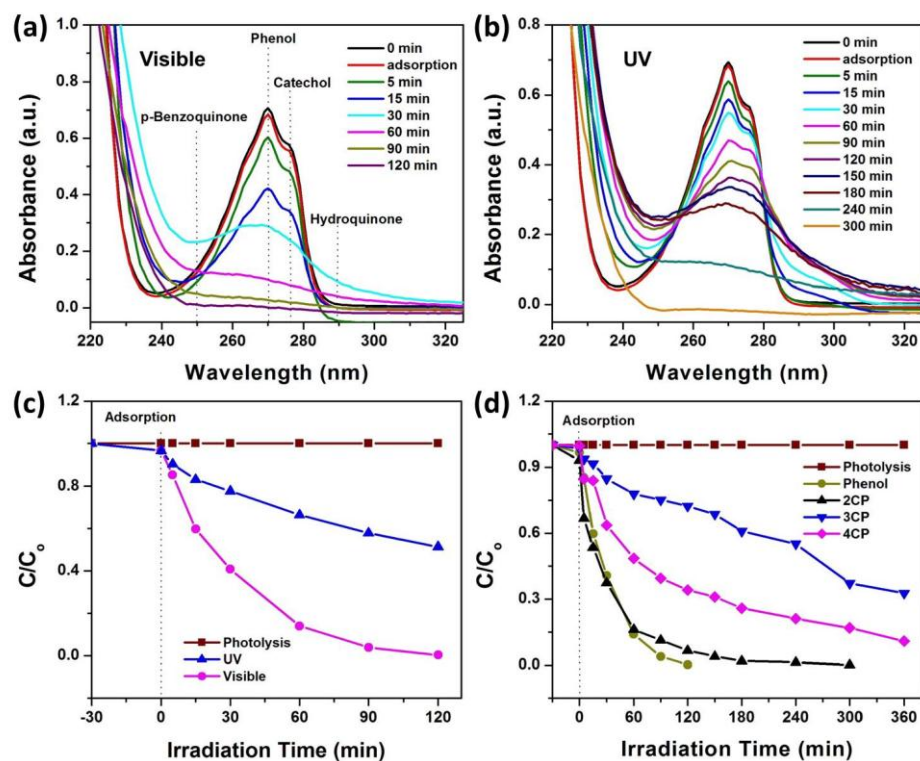
Figure 4A.1. UV-visible spectra for photocatalytic degradation of phenol under (a) visible and (b) UV light irradiation; (c) Photocatalytic degradation of phenol as a function of irradiation time under different light irradiation; (d) Photocatalytic degradation of various phenolic compounds as a function of irradiation time under visible light irradiation (Condition: $C_o = 0.5$ mM, $V = 20$ mL, catalyst amount = 10 mg, pH = 7).

It is observed that the degradation of phenol and its compounds follow the order: phenol>2CP>4CP>3CP. The corresponding UV-visible spectral changes for photodegradation of 2CP, 3CP and 4CP under visible light irradiation are shown in Figure 4A.2 (a, b and c). For 2CP, complete degradation (100%) has observed over ZnFe LDH in 300 min under visible light irradiation (Figure 4A.2d). While for 3CP and 4CP, % degradation of 67.4 and 89.1 have been observed, respectively in 360 min under visible light irradiation (Figure 4A.2d). Similar degradation order was also observed for phenol and its compounds under UV light irradiation. The corresponding changes of UV-visible spectral and % degradation for photodegradation of 2CP, 3CP and 4CP under UV light irradiation are shown in Figure A.3 (a, b, c and d, respectively) of Appendix. The % degradation values for all the phenolic compounds under different light irradiations are

presented in Table 4A.1. Thus, it is seen that ZnFe LDH exhibits efficient photocatalytic activity towards the degradation of phenol and its compounds under visible light irradiation. Blank experiments were also carried out without using any catalyst to check the stability of phenol and its compounds under different light irradiations. No significant changes in the concentration of phenol and its compounds have observed confirming that no photocatalytic degradation takes place in absence of the catalyst under various light irradiations. The corresponding UV-visible spectra for photocatalytic degradation of phenol and its compounds in absence of catalyst under visible light irradiation are shown in Figure A.4 of Appendix.
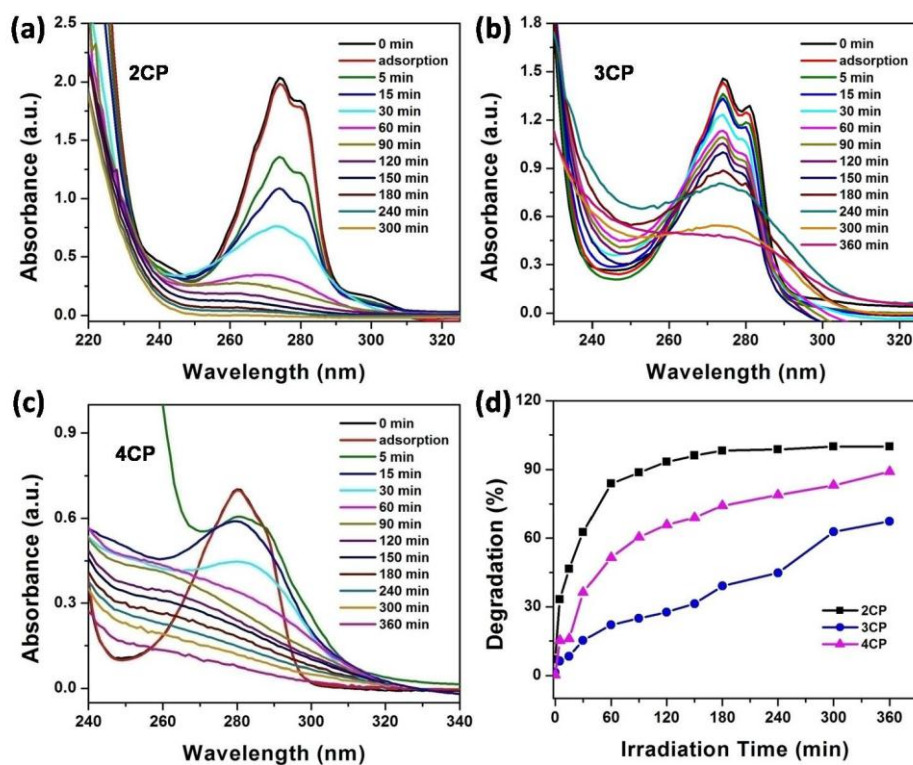
Figure 4A.2. UV-visible spectra for photocatalytic degradation of (a) 2CP, (b) 3CP and (c) 4CP; (d) Degradation (%) of 2CP, 3CP and 4CP with irradiation time over ZnFe LDH under visible light irradiation (Condition: C_o = 0.5 mM, V = 20 mL, catalyst amount = 10 mg, pH = 7).

4A.1.1 Optimization study

Optimization study was performed to effectively utilize the catalyst to get high efficiency for photodegradation at optimum catalyst amount, initial phenolic concentration and solution pH. First, the effect of catalyst amount on photodegradation of phenol and its compounds was studied under visible light irradiation. Here, we have varied the catalyst amount from 5 to 25 mg with constant initial phenolic concentration of 0.5 mM. Figure 4A.3 shows the % degradation of phenol and its compounds for photocatalytic degradation over ZnFe LDH with various catalyst amounts under visible light irradiation. It is observed that the % degradation of phenol and its compounds initially increases with increase in amount of the catalyst from 5 to 10 mg. This increase in % degradation can be attributed to the increased availability of the active catalytic sites upon increasing the catalyst concentration. Again, on performing the study by increasing the amount of catalyst to 15 and 20 mg, it is observed that no major changes in the % degradation has achieved even at higher catalyst concentrations for all case. This is because the active sites of the catalyst get saturated over higher catalytic dose resulting in lower of % degradation. Thus, the experimental results suggest that 10 mg is the optimum catalyst amount for photocatalytic degradation study.
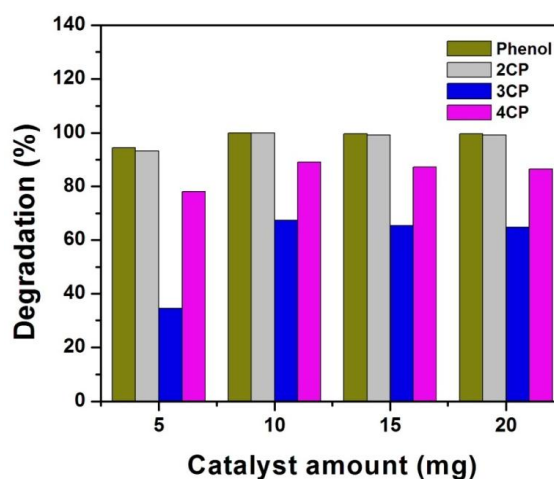

Figure 4A.3. Effect of amount of ZnFe LDH on photocatalytic degradation of phenol, 2CP, 3CP and 4CP under visible light irradiation (Condition: C_o = 0.5 mM, V = 20 mL, pH = 7).

The effect of initial concentration of phenol and its compounds on photocatalytic degradation was evaluated by varying concentrations of phenolic solutions at a fixed catalyst amount of 10 mg under visible light irradiation. Here, we have used five different concentrations of phenol and its compounds (0.1, 0.3, 0.5, 0.7 and 1 mM) to achieve an optimum phenolic concentration for photodegradation process. Figure 4A.4 shows the % degradation of phenol and its compounds at various initial concentrations under visible light irradiation. It is observed that maximum degradation is attained even upto higher concentration of 0.5 mM for all phenolic compounds. However, on increasing the concentration further upto 1 mM, decrease in the % degradation was observed. At higher concentrations, higher number of molecules is available for absorbing higher number of photons making them less available for reaching the catalyst surface required for initiating the photocatalytic reaction. As a result, decrease in % degradation of phenolic compounds is observed at higher initial concentrations. Therefore, we have selected 0.5 mM concentration as the optimum concentration for all phenolic compounds.
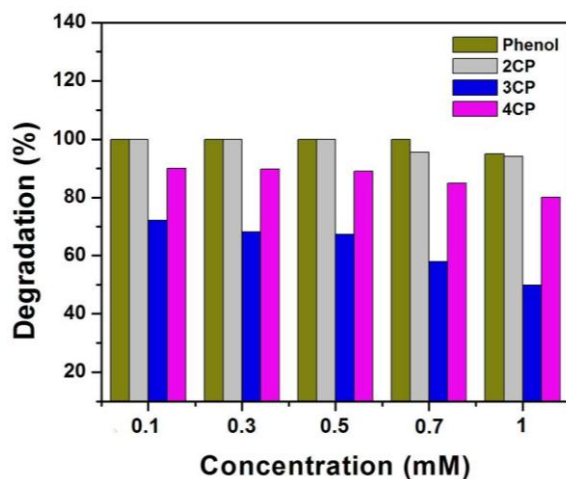
Figure 4A.4. Effect of initial concentration of phenol, 2CP, 3CP and 4CP on photocatalytic activity of ZnFe LDH for degradation under visible light irradiation (Condition: $V = 20$ mL, catalyst amount = 10 mg, pH = 7).

The pH of solution is another important factor for evaluating the photocatalytic degradation process with better efficiency. Effect of solution pH on photocatalytic degradation of phenol and its compounds was further studied by varying the pH in the ranges of 3–11 at a fixed phenolic concentration of 0.5 mM and catalyst amount of 10 mg

under visible light irradiation. The degradation efficiency of the catalyst for all the phenolic compounds at various pH is presented in Figure 4A.5. For all the compounds, it is observed that maximum degradation is obtained at neutral pH (pH 7). At lower pH (pH<7), the surface of the catalyst becomes highly positively charged and thus, prevent the dye molecules being adsorbed over the surface, resulting in decrease of photocatalytic efficiency of the catalyst. At higher pH (pH>7), the catalyst surface acquires more negative charges, leading to the higher adsorption of cationic dyes over its surface. This high adsorption dyes over the catalyst surface inhibits the light penetration and consequently, results in the decrease of photocatalytic activity of the catalyst. In acidic pH (pH<7), the % degradation is comparatively higher than in alkaline pH (pH>7).
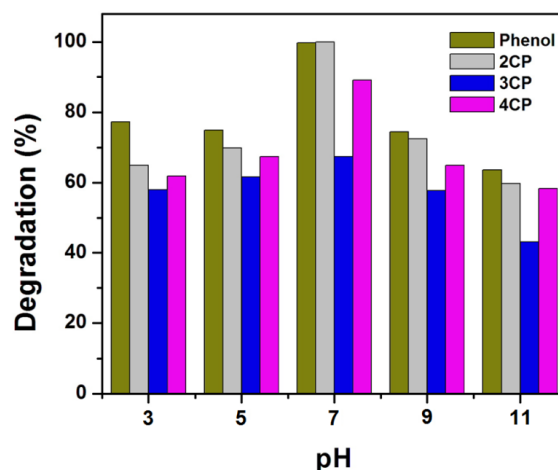

Figure 4A.5. Effect of pH on photocatalytic activity of ZnFe LDH for degradation of phenol and its compounds under visible light irradiation (Condition: $C_o = 0.5$ mM, $V = 20$ mL, catalyst amount = 10 mg).

4A.1.2 Reaction kinetics

The reaction kinetics for photocatalytic degradation of phenol and its compounds have been analyzed by using Langmuir–Hinshelwood first order kinetics (equation 2.19 of Chapter 2). The kinetic study was employed at a fixed phenolic concentration of 0.5 mM with catalyst amount of 10 mg at pH 7 under visible light irradiation and the results are shown in Figure 4A.6. The values of apparent rate constant, k_{app} for photocatalytic degradation of all the phenolic compounds have been calculated from the linear regression

of the plots of $\ln(C_o / C)$ *vs.* t which is a straight line with the slope, k_{app} and the values are presented in Table 4A.1.

Table 4A.1. % Degradation and pseudo first order kinetic parameters for photocatlytic degradation of phenol, 2CP, 3CP and 4CP over ZnFe LDH under different light irradiations.

Substrate	Light irradiation	Irradiation time (min)	% Degradation	k_{aap} (min^{-1})	R^2
Phenol	Visible	120	99.8	0.04957	0.98659
	UV	120	69.6	0.00904	0.99065
2CP	Visible	300	99.9	0.02348	0.98979
	UV	300	95.1	0.00874	0.94033
3CP	Visible	360	67.4	0.00289	0.98297
	UV	360	58.6	0.00211	0.98491
4CP	Visible	360	89.1	0.00565	0.97936
	UV	360	79.3	0.00447	0.95853

The correlation coefficient value, R^2 determined *via* linear regression of the plots confirms that the degradation of phenol and its compounds follows a first order kinetics model with $R^2 > 0.9$ for each case (Figure 4A.6 and Table 4A.1). The calculated k_{app} values are 0.04957, 0.02348, 0.00289 and 0.00565 min^{-1} for phenol, 2CP, 3CP and 4CP, respectively. The k_{app} values are in accordance with the enhanced photocatalytic activity of the catalyst for degradation of various phenolic compounds under visible light irradiations with degradation trends following: Phenol>2CP>4CP>3CP. For comparison, the kinetics study was also carried out under UV light irradiation and corresponding $\ln(C_o / C)$ *vs.* t plots for all the phenolic compounds are shown in Figure A.5 of Appendix. The calculated k_{app} and R^2 values for degradation under UV light are given in Table 4A.1.
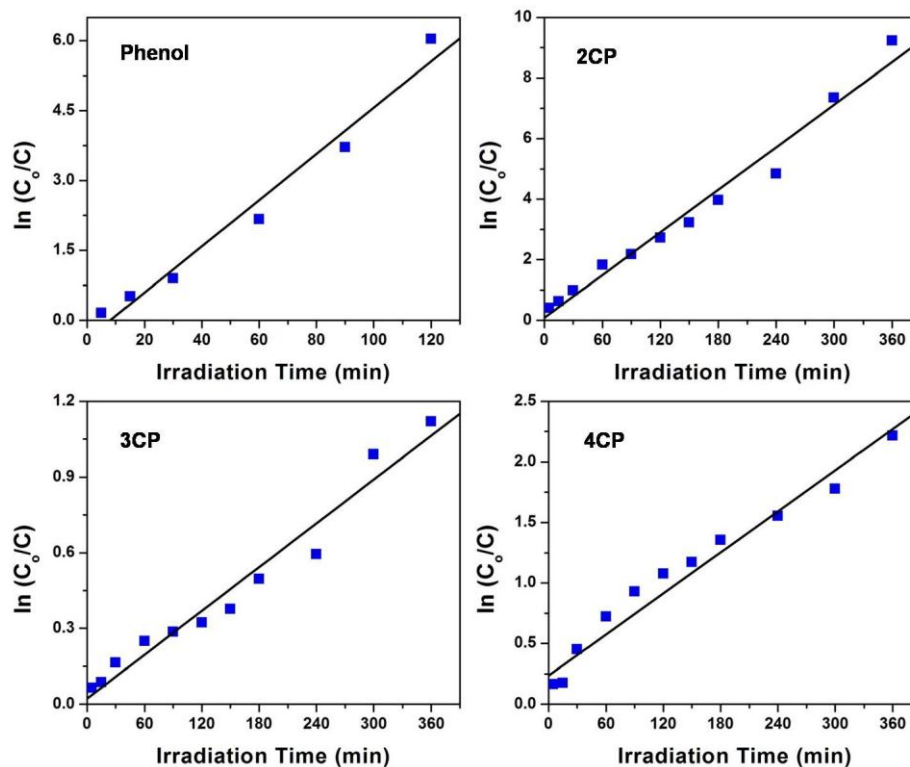
Figure 4A.6. Pseudo-first order kinetic plots for photocatalytic degradation of phenol, 2CP, 3CP and 4CP over ZnFe-LDH under visible light irradiation (Condition: $C_o = 0.5$ mM, $V = 20$ mL, Catalyst amount = 10 mg, pH = 7).

Thus, ZnFe LDH is considered as a highly efficient and economic photocatalyst towards the removal of harmful organic pollutants. Tzompantzi *et al.* [37] reported the photocatalytic degradation of phenolic compounds using ZnAl derived mixed oxides using UV light irradiation and the catalyst exhibited about 95% degradation of phenol in 4h. Valente *et al.* [38] demonstrated the photocatalytic degradation of phenol and chlorinated phenols using CeO_2 supported MgAl LDH under UV light irradiation and achieved 50% degradation for phenol in 7h and 96% degradation for 4-chlorophenol in 5h. Dixit *et al.* [39] reported the photo oxidation of phenol and 4-chlorophenol using TiO_2 as photocatalyst using H_2O_2 as oxidant under UV light irradiation and the results showed maximum degradation of 74.6 and 79.8% for phenol and 4-chlorophenol, respectively within 90 min.

4A.1.3 Proposed mechanism and degradation pathways

The enhanced photocatalytic activity of ZnFe LDH can be understood in terms of various facts which include the presence of surface hydroxyl groups (–OH), interlayer carbonate anions, band gap energy and photoactive Zn metal in the LDH structure. The proposed mechanism for photocatalytic degradation of phenol over ZnFe-LDH is schematically presented in Figure 4A.7. When the catalyst is subjected to light irradiations, photons with energy (hv) equal to or greater than the band gap of the catalyst excite the electrons from valence band to the conduction band leaving behind positive holes (h^+) in the valence band and thus the pairs of positive hole and negative electron are generated to promote the degradation process [40,41].
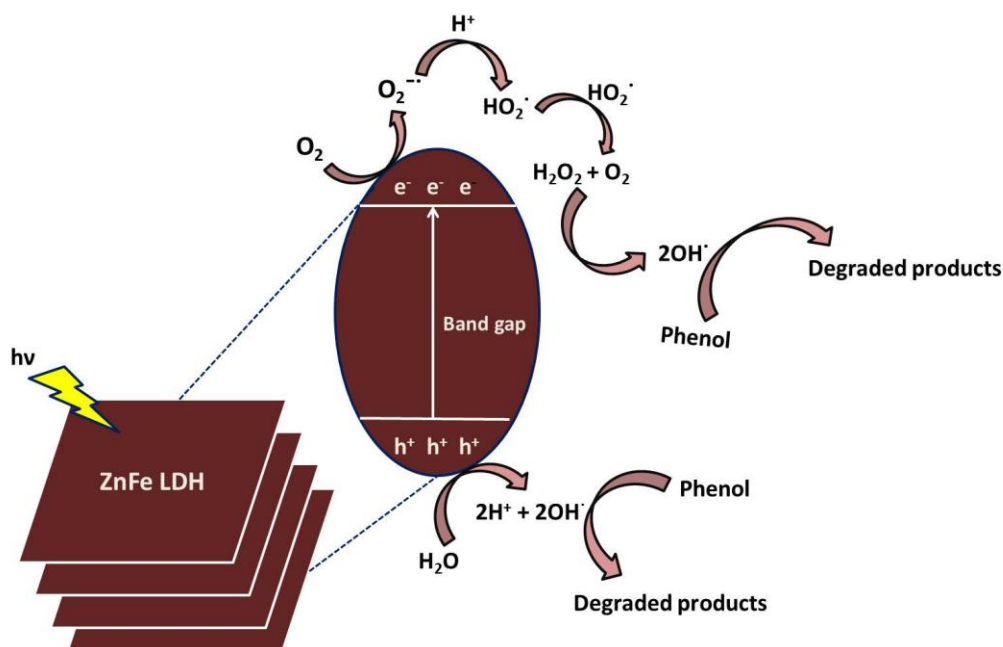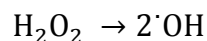

Figure 4A.7. Schematic diagram of the proposed mechanism for photocatalytic degradation of phenol over ZnFe-LDH.

The H_2O molecules in the reaction medium combine with the positive holes in the valence band and generates $^•OH$ radicals. The adsorbed O_2 molecule on the catalyst surface form superoxide radicals, $O_2^{•-}$ by combining with the photogenerated negative electrons in the conduction band. The $O_2^{•-}$ radicals thus formed again combine with H^+ ions and generates $HO_2^•$ radicals which in return combining with the another molecules of $HO_2^•$ radicals result in the formation of H_2O_2. This *insitu* generated H_2O_2 finally form the oxidizing species,

˙OH radicals which are mainly considered as the active species for initiating the degradation of phenolic compounds. Thus, the presence of surface –OH group in the LDH structure also adds up to the enhanced photocatalytic activity of the catalyst with the formation of ˙OH radicals by combining with photogenerated positive holes in the valence band, inhibiting the recombination of positive holes and negative electrons [34,42]. The presence of intercalated carbonate anions in the LDH structure also play an important role in the enhanced degradation of phenolic compounds by inhibiting the recombination of photogenerated positive holes and negative electrons [43]. Moreover, due to synergetic effect, carbonate intercalated LDH exhibit stronger photoabsorption properties resulting in the enhanced photocatalytic activity of the LDH [41]. The optimum band gap energy of the photocatalyst also plays an important role in the enhanced photocatalytic activity by increasing the electron hole pair generation [44]. The overall possible degradation mechanism for photocatalytic degradation of phenol and its compounds over ZnFe LDH can be expressed as follows,

$$ZnFeLDH + hv \rightarrow h^+ + e^-$$
$$H_2O + h^+ \rightarrow 2^\cdot OH + 2H^+$$
$$O_2 + e^- \rightarrow O_2^{\cdot-}$$
$$O_2^{\cdot-} + H^+ \rightarrow HO_2^\cdot$$
$$HO_2^\cdot + HO_2^\cdot \rightarrow H_2O_2 + O_2$$
$$H_2O_2 \rightarrow 2^\cdot OH$$
$$^\cdot OH + \text{Phenolic compounds} \rightarrow \text{Degraded products}$$
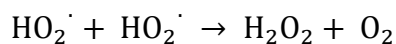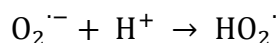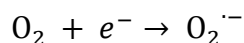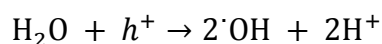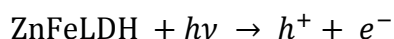
The phenol degradation proceeds via the formation of various transient states such as catechol and hydroquinone and it is clearly understood from the UV-vis spectra of phenol degradation (Figure 4A.1a). These transient states further undergo to the aromatic ring opening resulting the subsequent formation of various aliphatic compounds such as maleic acid and oxalic acid; and finally resulting in the mineralization of the toxic organic contaminants into less toxic products such as CO_2 and H_2O; and also Cl^- in case of chlorophenols [45–47]. We performed DFT calculations in systematic manner to understand the mechanism of phenol degradation. The proposed degradation pathways

for photocatalytic degradation of phenol over ZnFe LDH initiated by ˙OH radical based on our experimental and DFT calculations are presented in the Figure 4A.8.
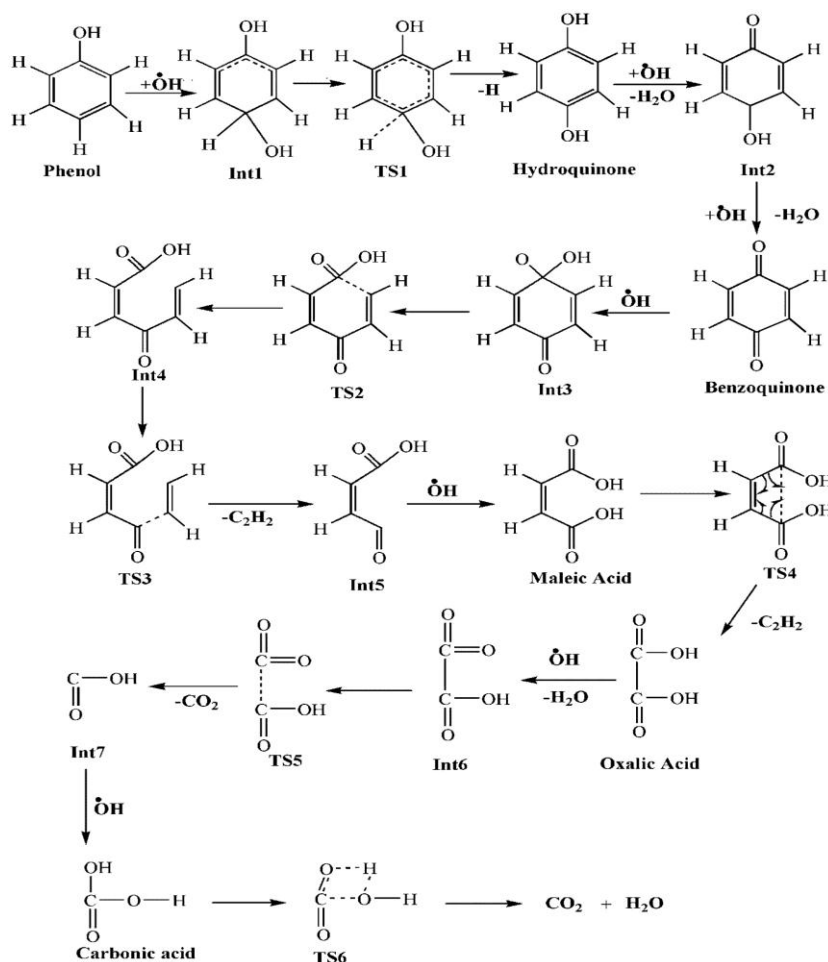
Figure 4A.8. Proposed degradation pathway for photocatalytic degradation of phenol initiated by ˙OH radical.

4A.2   DFT investigation of Phenol + ˙OH reaction

4A.2.1   Electronic structures and vibrational frequency analysis

The optimized structures of all species along with bond length (Å) given in Figure 4A.8 are obtained at DFT (B3LYP)/6-31+G(d,p) level of theory as shown in Figure 4A.9. It is obvious from Figure 4A.9 that a conversion of phenol into hydroquinone in the presence of ˙OH radical goes through Int.1 and TS1. In Int.1, the length the C–H bond which is disintegrating measures 1.105 Å and the C–O bond formed measures 1.462 Å, respectively.

Figure 4A.9. Optimized structures of all species involved in the Phenol + ˙OH reaction at B3LYP/6-31+G(d,p) level of theory.

In TS1, the variation in C–H bond length which is broken in course of the reaction shows an increase from 1.105 to 1.806 Å and the C–O bond which is forming shows a decrease from 1.462 to 1.382 Å with respect to Int.1. In the optimized geometry of hydroquinone, C–O bond further decreases from 1.382 to 1.376 Å with respect to TS1. We have also obtained stable Int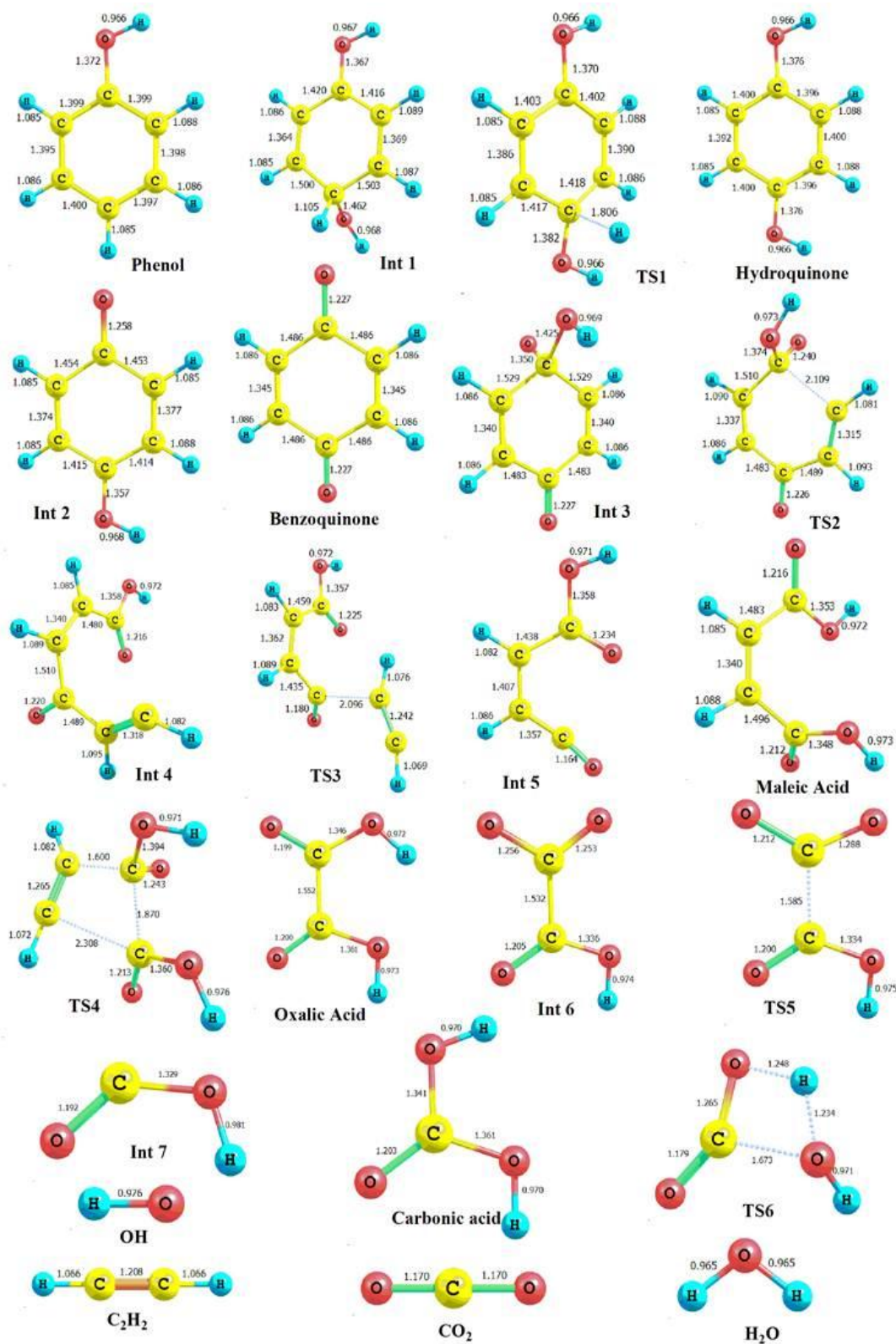.2, an optimized structure in between hydroquinone and benzoquinone. In this conversion two successive addition of ˙OH radicals and release of two water molecules have occurred. After that a ring opening process takes place and formation of maleic acid occurs via three stable intermediates (Int.3–Int.5) and two transition states (TS2 and TS3). We added ˙OH radical to one –CO group of benzoquinone and got stable Int.3 structure in which C–C bond increases from 1.486 to 1.529 Å with respect benzoquinone. Then TS2 structure is obtained in which C–C bond breaks and consequently an Int.4 structure is obtained. In the next step, another C–C bond again breaks in Int.4 to give Int.5 + C_2H_2 via TS3. We further added one ˙OH radical in Int.5 and formed maleic acid. After that oxalic acid and C_2H_2 are obtained via TS4. The magnitude of electronic energy of TS4 is very high owing to the breakage of two C–C bonds. Oxalic acid is then converted into Int.7 + CO_2 + H_2O via Int.6 and TS5. Finally one ˙OH radical added to Int.7 to form carbonic acid which converted into CO_2 + H_2O via TS6. The values of vibrational frequencies of all the species including transition states are obtained during frequency calculation done at the same level of theory. It is observed from frequency calculations that all the species correspond to local minima having real positive vibrational frequencies except transition states. Transition state structures TS1, TS2, TS3, TS4, TS5 and TS6 are characterized by the presence of only one imaginary frequency at $836i$ cm^{-1}, $387i$ cm^{-1}, $653i$ cm^{-1}, $452i$ cm^{-1}, $550i$ cm^{-1} and $1704i$ cm^{-1}, respectively. We have visualized the imaginary frequency vibrations of the transition states using ChemCraft program [48]. To validate the smooth connection of transition state with reactants and products, intrinsic reaction coordinate (IRC) calculations are also performed for TSs at the same level of theory. After frequency calculation, we have obtained thermochemistry data which are utilized to check the feasibility of the reaction channel. The standard reaction enthalpy ($\Delta_r H^0$) and Gibbs free energy ($\Delta_r G^0$) for the three reaction channel of same reaction have been calculated. These values are given in the Table 4A.2.

Table 4A.2. Reaction enthalpy ($\Delta_r H^0$) and Gibbs free energy ($\Delta_r G^0$) for the photocatalytic degradation of phenol.

Reaction Channel	$\Delta_r H^0$ (kcal/mol)	$\Delta_r G^0$ (kcal/mol)
Phenol + 3˙OH → Bezoquinone + H˙ + 2H$_2$O	-84.96	-83.33
Bezoquinone + 2˙OH → Oxalic acid + 2C$_2$H$_2$	-38.71	-41.70
Oxalic Acid + 2˙OH → 2CO$_2$ + 2H$_2$O	-142.03	-151.34

Table 4A.3. Total energy (Hartree) and relative energies (kcal/mol) of all species involved in the reaction calculated at B3LYP/6-31+G (d,p) levels of theory.

Reaction Channel	E_0 (Hartree)	RE(kcal/mol)
Phenol + 3˙OH	-534.5859275	0
Int1 + 2˙OH	-534.6069423	-13.19
TS1 + 2˙OH	-534.5659863	12.52
Hydroquinone + H˙ +2˙OH	-534.5741547	7.39
Int2 + H$_2$O + H˙ + ˙OH	-534.6334004	-29.79
Benzoquinone + H˙ + 2H$_2$O	-534.7219417	-85.35
Benzoquinone + 2˙OH	-532.8563891	0
Int3 + ˙OH	-532.8694223	-8.18
TS2 + ˙OH	-532.8498191	4.12
Int4 + ˙OH	-532.8653829	-5.64
TS3 + ˙OH	-532.8293869	16.94
Int5 + C$_2$H$_2$ + ˙OH	-532.8585253	-1.34
Maleic Acid + C$_2$H$_2$	-532.990904	-84.41
TS4 + C$_2$H$_2$	-532.7962681	37.73
Oxalic Acid + 2C$_2$H$_2$	-532.9183817	-38.90
Oxalic Acid + 2˙OH	-529.7575785	0
Int6 + H$_2$O + ˙OH	-529.7764972	-11.87
TS5 + H$_2$O + ˙OH	-529.7745803	-10.67
Int7 + CO$_2$ + H$_2$O + ˙OH	-529.8101151	-32.97
Carbonic Acid + CO$_2$ + H$_2$O	-529.9745417	-136.15
TS6 + CO$_2$ + H$_2$O	-529.9131231	-97.61
2CO$_2$ + 2H$_2$O	-529.985534	-143.04

The values of $\Delta_r H^0$ and $\Delta_r G^0$ for the reaction channels are found to be negative which indicates the feasibility of the reaction channels. We have also characterized all stationary points (both minima and saddle points) on the potential energy surface (PES). Total energy (E_{ele} + ZPE) of all species are required in order to plot PES diagram. Therefore, we have reported total energy (Hartree) along with relative energies with respect to Phenol + 3˙OH, Bezoquinone + 2˙OH and Oxalic Acid + 2˙OH at B3LYP/6-31+G (d,p) level of theory in Table 4A.3.

The potential energy diagram of the Phenol + ˙OH reaction is shown in Figure 4A.10, which constructed with the data given in Table 4A.3.
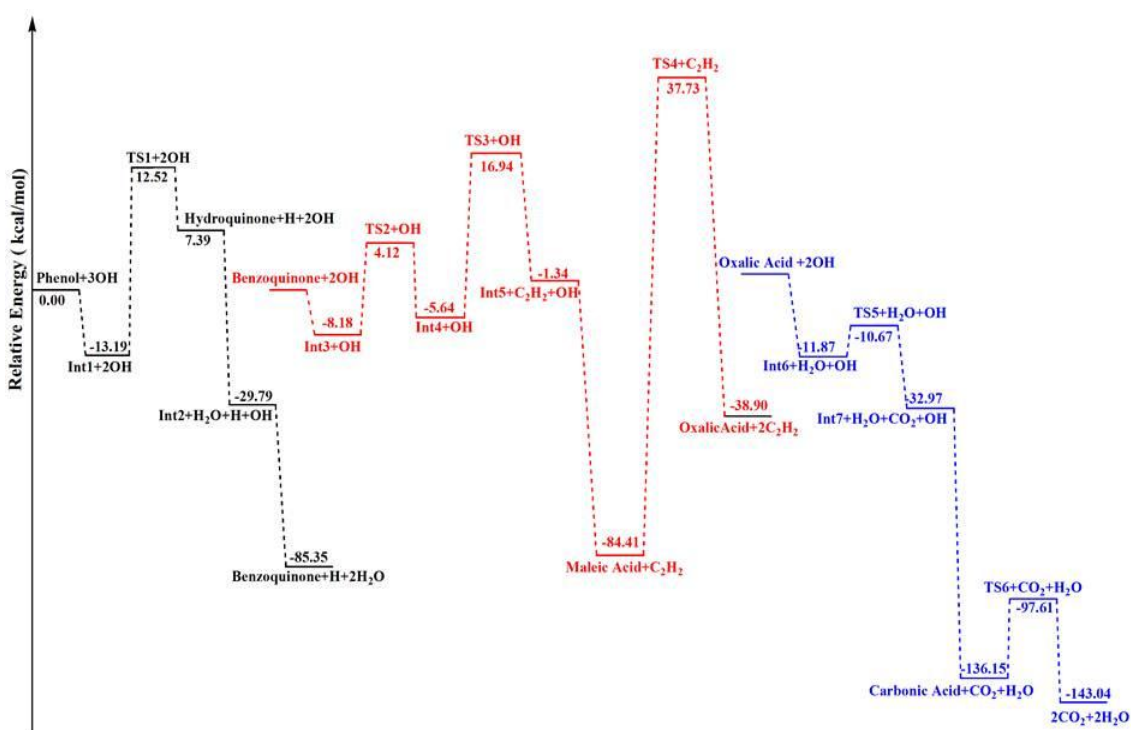
Figure 4A.10. Potential energy surface (PES) diagram for the degradation of Phenol + ˙OH reaction at B3LYP/6-31+G(d,p).

We have plotted PES diagram for Phenol + ˙OH reaction in three steps (i.e. Phenol + 3˙OH → Benzoquinone + 2H$_2$O, Benzoquinone + 2˙OH → Oxalic acid + 2C$_2$H$_2$ and Oxalic acid + 2˙OH → 2CO$_2$ + H$_2$O) as shown by black, red and blue color. This diagram gives information about kinetic and thermodynamic feasibility of degradation of Phenol + ˙OH reaction.

4A.3   Recyclability of ZnFe LDH

Recyclability of catalyst is an important factor in terms of practical point of view to achieve high efficiency even after long term applications. The recyclability of the catalyst was tested for phenol degradation under visible light irradiation using similar experimental conditions and displayed in Figure 4A.11. After each run, the used catalyst was separated from the solution by filtration and washed thoroughly with distilled water followed by ethanol. After properly washing, the catalyst was dried overnight at 80 °C in oven and again subjected for a new run. The catalyst shows % degradation above 90% upto four successive cycles suggesting very small or negligible loss in the catalytic activity of the catalyst towards the photodegradation of phenol in each cycle.
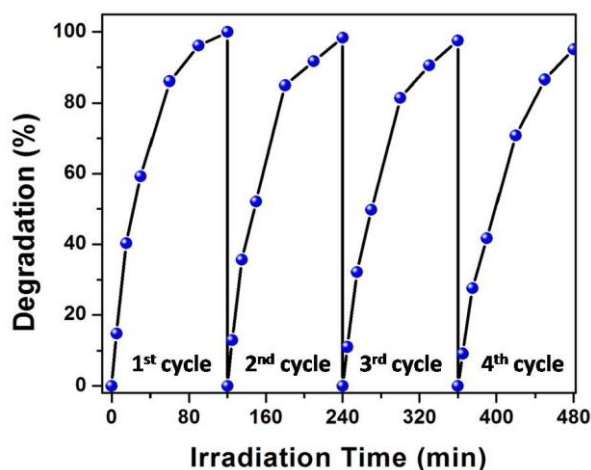
Figure 4A.11. Recyclability of ZnFe LDH for photocatalytic degradation of phenol under visible light irradiation.

In summary, ZnFe LDH synthesized via co-precipitation method have employed as a photocatalyst towards the degradation of various phenolic compounds including chlorophenols under visible and UV light irradiations. The catalyst shows efficient activity for phtodegradation of phenolic compounds under visible light. The effect of various parameters such as catalyst amount, initial concentration of phenolic compounds and solution pH on photodegradation process has been studied. The photodegradation process follows Langmuir-Hinshelwood first order kinetics for all the phenolic compounds. The degradation proceeds via aromatic ring opening leading to the formation

of corresponding aliphatic acids and finally to mineralized products. Moreover, the phenolic degradation pathway is well supported by theoretical study. The recyclability test for phenol degradation shows that the photocatalyst could be reused upto four successful cycles.

Section 4B: Photocatalytic degradation of methylene blue and rhodamine B using ZnFe layered double hydroxide

In this section, we have discussed the photocatalytic degradation of organic dye pollutants such as methylene blue (MB) and rhodamine B (RhB) in aqueous solution using ZnFe LDH under both UV and visible light irradiations.

4B.1   Photocatalytic degradation of MB and RhB

The catalytic activity of ZnFe LDH has been investigated for photodegradation of MB and RhB under UV and visible light irradiations. The stability of MB and RhB under both UV and visible light irradiations was first tested by employing blank experiments in absence of any catalyst. In absence of catalyst, photolysis reactions take place with very small or negligible amount of degradation for MB and RhB demonstrating the stability of the dyes under different light irradiations. Prior to subject for photodegradation under different light irradiations, the dye solutions of MB and RhB were kept in dark for 120 and 240 min, respectively to achieve an adsorption-desorption equilibrium. An equilibrium state of adsorption has been achieved within 30 min with % dye adsorption of 4.5 and 2.9% for MB and RhB, respectively (Figure 4B.1). Thus, it is observed that in absence of a catalyst and light source, very small or negligible degradation of dyes are attained. Therefore, it is necessary to expose the dye suspensions with an effective photocatalyst under light illuminations for efficient degradation to occur.

4B.1.1 Degradation of MB and RhB under UV light irradiation

The dye suspensions (MB and RhB) were first subjected to expose under UV light irradiation for photocatalytic degradation process. Figure 4B.1 shows the photolysis, adsorption and photodegradaton of MB and RhB under UV light irradiation as function of concentration and irradiation time. It is seen that the concentration of dye goes on decreasing with irradiation time and reaches almost zero in 120 and 240 min, indicating excellent photocatalytic activity of the catalyst. The catalyst exhibits degradation of 99.9 and 99.8% for MB and RhB, respectively under UV light irradiation (Table 4B.1 and Figure A.6 of Appendix).

Figure 4B.1. Photolysis, adsorption and photocatalysis of MB and RhB over ZnFe LDH under UV light irradiation (Conditions: C_o = 10 mg/L, $V_{solution}$ = 50 mL, catalyst amount = 5 mg for MB and 10 mg for RhB, pH = 7).
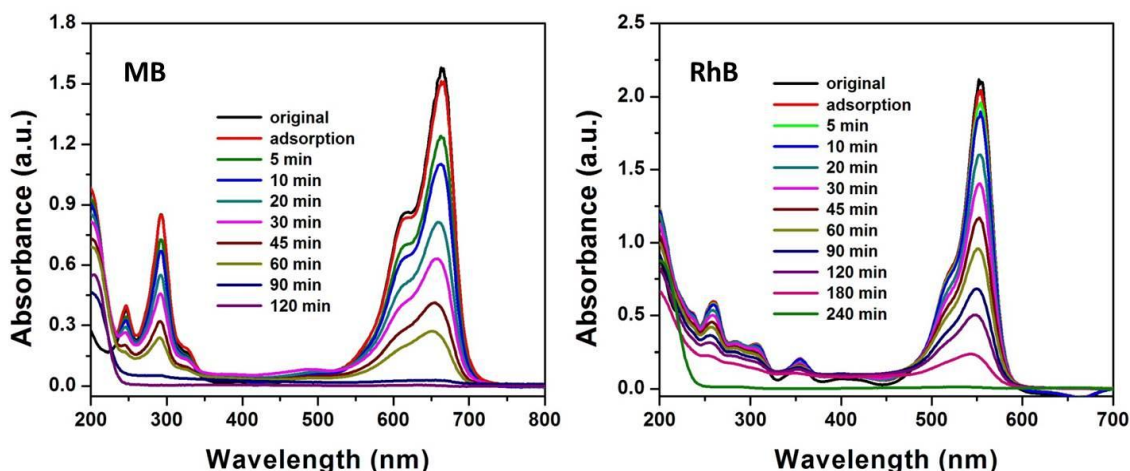
Figure 4B.2. UV-visible spectra for phocatalytic degradation of MB and RhB over ZnFe LDH under UV light irradiation (C_o = 10 mg/L, $V_{solution}$ = 50 mL, catalyst amount = 5 mg for MB and 10 mg for RhB, pH = 7).

The corresponding UV-vis spectral changes for photodegradation of MB and RhB under UV light irradiation are presented in Figure 4B.2. The characteristic UV-vis adsorption peaks of the dyes (λ_{max} = 663 and 554 nm for MB and RhB, respectively) gradually decease with time indicating step by step degradation of aromatic rings of the dye molecules upon exposure to light. Finally, the peaks get diminished completely demonstrating the complete degradation of dyes under UV light irradiations.

Table 4B.1. Degradation (%), K_{app} and linear regression value for photodegradation of MB and RhB over ZnFe LDH under UV light irradiation.

Dye	Degradation (%)	K_{app} (min^{-1})	R^2
MB	99.9	0.033	0.992
RhB	99.8	0.0162	0.996

4B.1.2 Degradation of MB and RhB under visible light irradiation

The photocatalytic degradation of MB and RhB were also tested by exposing under visible light irradiation. Figure 4B.3 shows the photolysis, adsorption and photocatalysis of MB and RhB in terms of concentration and irradiation time under visible light irradiation. The photolysis and adsorption show negligible changes in the dye concentrations. The photocatalytic study shows that the degradation process is slow for both cases and it can be clearly depicted from the Figure 4B.3.
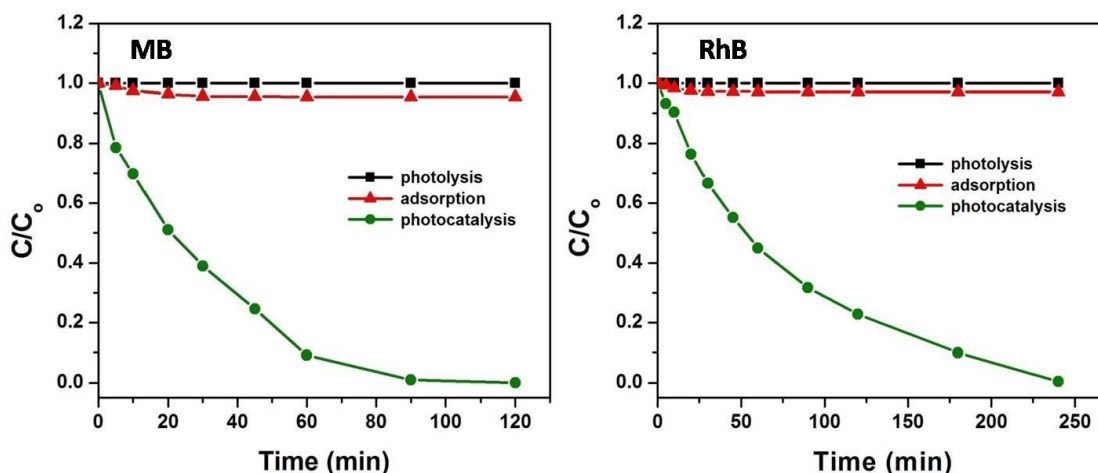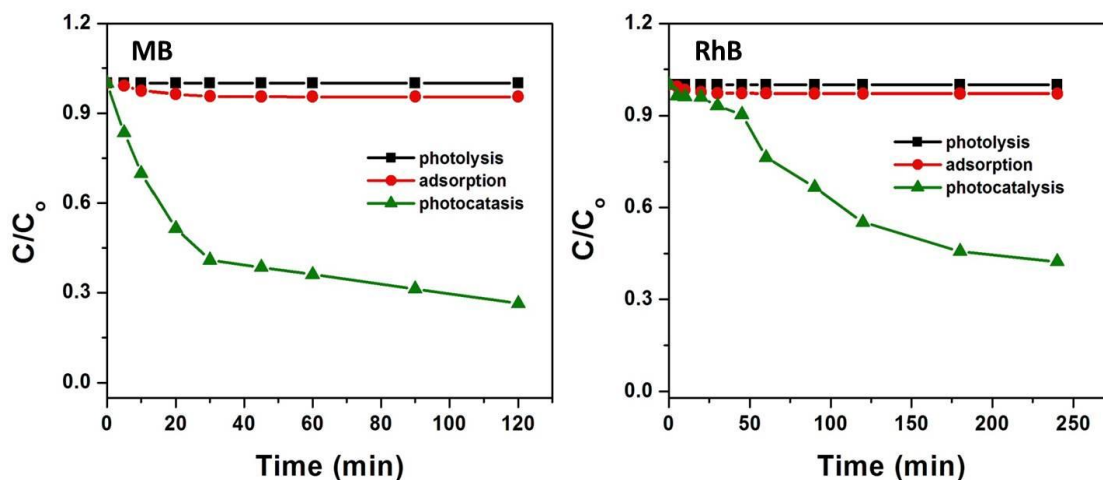

Figure 4B.3. Photolysis, adsorption and photocatalysis of MB and RhB over ZnFe LDH under visible light irradiation (Conditions: $C_o = 10$ mg/L, $V_{solution} = 50$ mL, catalyst amount = 5 mg for MB and 10 mg for RhB, pH = 7).

Slow decreases in the concentration of dyes are observed for both dyes with time indicating that degradations are not completed within the specified time as in case of degradation under UV light irradiation. The catalyst exhibits % degradation of only 73.6

and 57.7% in 120 and 240 min for MB and RhB, respectively under visible light irradiation (Figure A.6 of Appendix). The corresponding UV-vis spectral changes for photodegradation of MB and RhB under visible light irradiation are presented in Figure 4B.4. Thus, the catalyst shows efficient photocatalytic activity towards the photodegradation of MB and RhB under UV light compared to visible light irradiation.
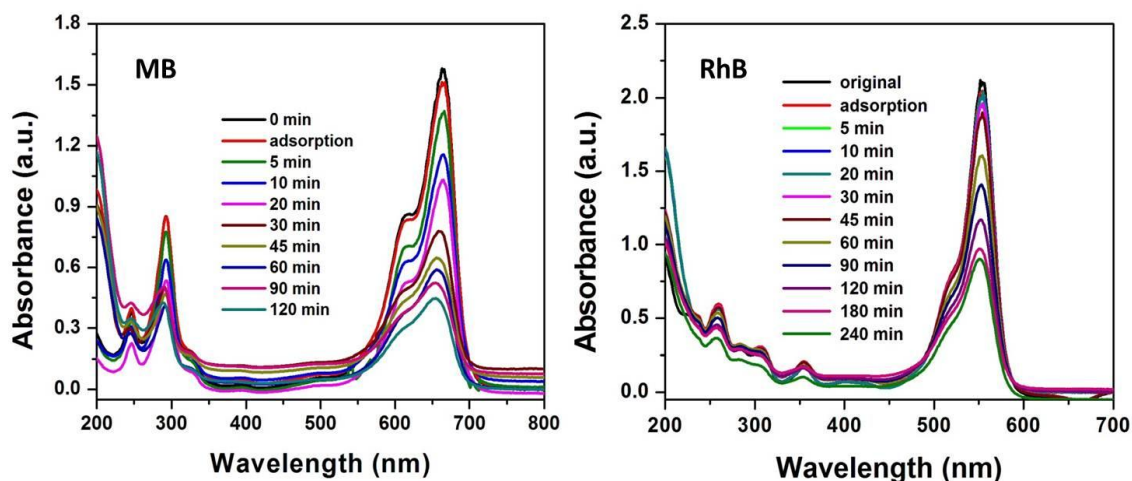
Figure 4B.4. UV-visible spectra for phocatalytic degradation of MB and RhB over ZnFe LDH under visible light irradiation (C_o = 10 mg/L, $V_{solution}$ = 50 mL, catalyst amount = 5 mg for MB and 10 mg for RhB, pH = 7).

4B.1.3 Optimization study

The optimization study has been carried out to efficiently utilize the catalyst at an optimum range towards the photocatalytic degradation of MB and RhB under UV light irradiation. The effects of various parameters such as catalyst amount, dye concentration and pH of dye solutions on the photodegration process were studied. The photocatalytic degradation of MB and RhB was studied with different catalyst amount for a fixed dye concentration of 10 mg/L under UV light irradiation and are shown in Figure 4B.5. To determine the optimum catalyst amount for photodegradation of MB, four different catalyst amounts of 3, 5, 7 and 10 mg were used. In case of MB, it is observed that the degradation gradually increases from 96 to 100% upon increasing the catalyst amount from 3 to 5 mg in 120 min. Again, on increasing the catalyst amount upto 10 mg, no considerable change in the degradation as a function of time is observed. The only

observable difference is that at higher catalyst amount (10 mg), the % dye degradation quickly increases first and reaches maximum degradation as in case of 5 and 7 mg catalyst amount. Therefore, we have selected 5 mg as optimum catalyst amount for MB degradation. Similarly, in case of RhB, when the catalyst amount is increased from 3 to 5 mg, RhB degradation quickly increases from 81 to 90%. Again, on increase in catalyst amount upto 10 mg, complete degradation of RhB is observed in 240 min. Therefore, we have selected 10 mg as optimum catalyst amount for RhB degradation.

Figure 4B.5. Effect of catalyst amount on photocatalytic degradation of MB and RhB with irradiation time under UV light irradiation (Conditions: C_o = 10 mg/L, $V_{solution}$ = 50 mL, catalyst amount = 5 mg for MB and 10 mg for RhB, pH = 7).

The photocatalytic degradations of MB and RhB were further studied by varying the initial dye concentrations with a fixed catalyst amount (5 and 10 mg for MB and RhB, respectively) at pH 7 under UV light irradiation. Four different dye concentrations of 5, 7, 10 and 12 mg/L were used for both cases and the results are presented in Figure 4B.6. It is observed that the % degradation decreases as the initial concentration of dyes increases from 5 to 12 mg/L. This is because more of the photons get adsorbed by dye molecules resulting in the unavailability of the required amount of photons to reach the catalyst surface for degradation process. Thus, we have selected 10 mg/L as optimum concentration for both cases.

Figure 4B.6. Effect of initial dye concentrations on photocatalytic degradation of MB and RhB with irradiation time under UV light irradiation (Conditions: $V_{solution}$ = 50 mL, catalyst amount = 5 mg for MB and 10 mg for RhB, pH = 7).

The solution pH is an important factor influencing the photodegradation efficiency [49]. To find the optimal pH for photo degradation process, the experiments were carried out at a fixed MB and RhB concentrations (10 mg/L). The catalyst amounts were 5 and 10 mg for MB and RhB, respectively. Here, we have varied the pH of the dye solutions from 3 to 11. Figure 4B.7 shows a comparative study for degradation of MB and RhB as a function of pH. It is observed that for both cases, the photocatalytic efficiency for degradation of dyes (MB and RhB) under UV light irradiation is highest at pH 7. In lower pH (pH<7), the catalyst surface is highly positively charged preventing the adsorption of dye over the catalyst surface resulting the decrease in percentage of degradation. At higher pH (pH>7), the surface of the catalyst become more negatively charged leading to the higher adsorption of cationic dyes on the catalyst surface. This high adsorption dyes on catalyst surface inhibits the light penetration and consequently results in the decrease in percentage of degradation.
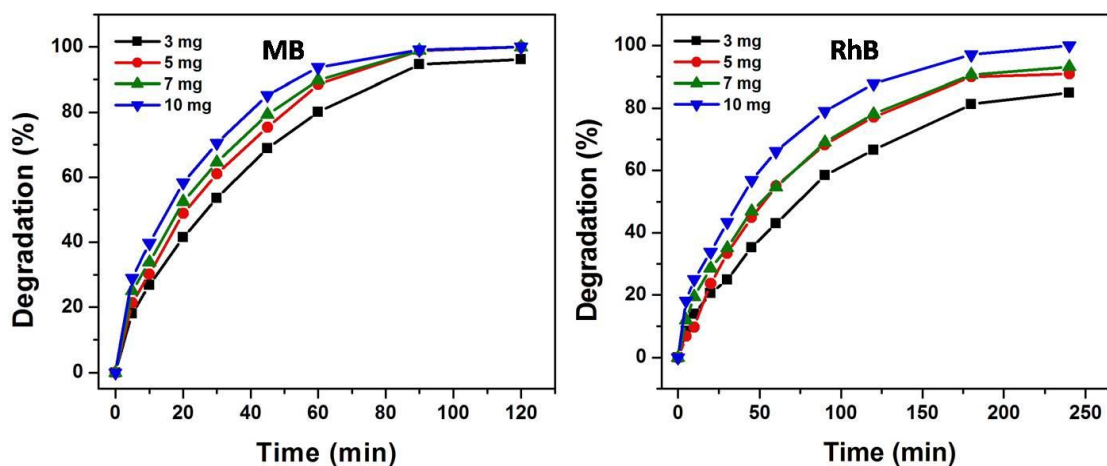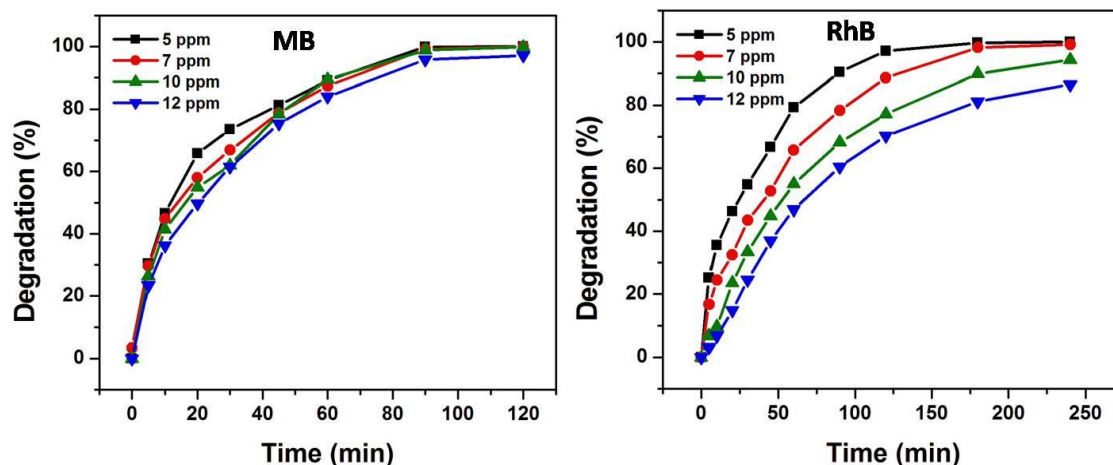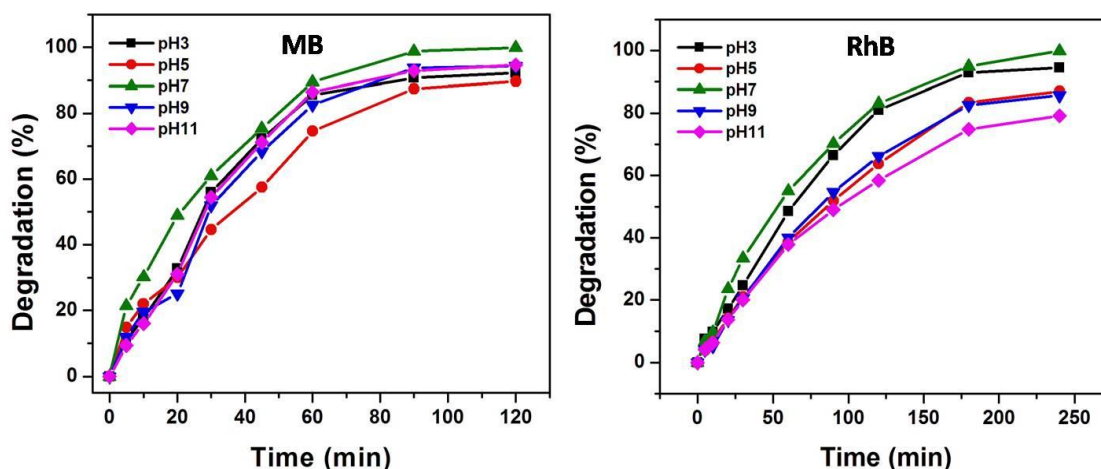
Figure 4B.7. Effect of pH on photocatalytic degradation of MB and RhB with irradiation time under UV light irradiation (Conditions: C_o = 10 mg/L, $V_{solution}$ = 50 mL, catalyst amount = 5 mg for MB and 10 mg for RhB).

4B.1.4 Reaction kinetics

The kinetics for photocatalytic degradation of MB and RhB over ZnFe LDH were analyzed using 10 mg/L of respective dye solutions with 5 and 10 mg catalyst amount for MB and RhB, respectively at pH 7. The degradation kinetics follows Langmuir-Hinshelwood first-order kinetics and is expressed by equation 2.19.
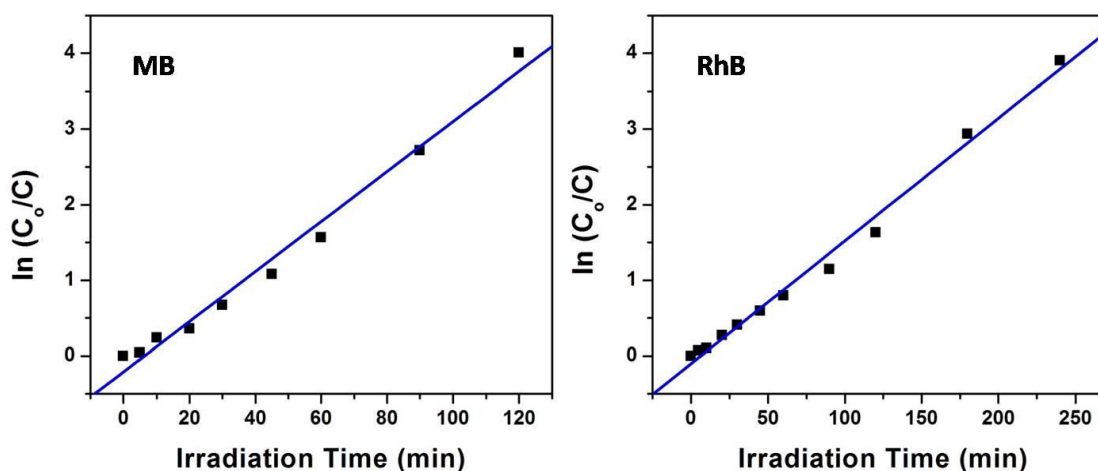
Figure 4B.8. Kinetic plots of ln (C_o/C) as a function of time for photodegradation of MB and RhB under UV light irradiation.

The variations of $\ln\left(\frac{C_o}{C}\right)$ as a function of light irradiation time for photocatalytic degradation of MB and RhB under UV light irradiation are shown in Figure 4B.8. The value of apparent rate constant, K_{app} has been calculated from the slope of the plot of $\ln\left(\frac{C_o}{C}\right)$ versus t. The corresponding values of linear regression (R^2) are 0.992 and 0.996 with K_{app} values 0.033 and 0.0162 for MB and RhB, respectively (Table 4B.1). Thus the R^2 values show better fitting of kinetic data with first order model, demonstrating that the degradation process follows first order kinetics for both cases (R^2>0.99).

4B.1.5 Proposed degradation mechanism

For photocatalytic reaction, the initial step is the activation of the catalyst in presence of higher energy radiation (energy greater than or equal to ba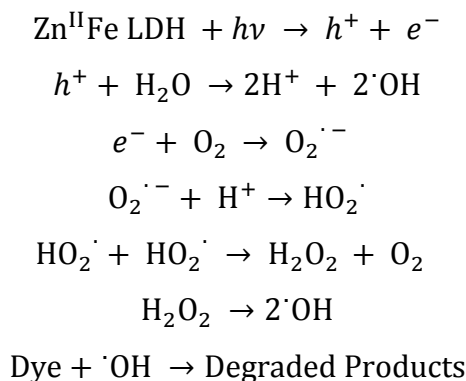nd gap energy). When the catalyst, ZnFe LDH absorbs light radiation, a pair of photo generated electrons and holes (e^-–h^+) get produced. The positive holes (h^+) of the catalyst combine with the water molecule and break it to form hydroxyl radical ($^\bullet$OH). The negative electrons (e^-) form highly oxidizing superoxide radicals ($O_2^{-\bullet}$) by combining with the dioxygen. The $O_2^{-\bullet}$ then combining with H^+ ion generates highly active $HO_2^\bullet$ radical and finally resulting in the formation of highly oxidizing species, such as $^\bullet$OH radicals through the formation of H_2O_2. The surface hydroxyl groups present in the LDH structure also play a significant role in the degradation process by capturing the positive holes (h^+) so that recombination of the hole and electron do not take place leading to the enhanced activity of the catalyst for photodedegradation [31,41]. Thus, the e^-–h^+ pair mechanism is an important factor enhancing the photocatalytic performance. Moreover, the enhanced photocatalytic activity of ZnFe LDH is due to the presence of intercalated carbonate anions. The carbonate intercalated LDHs exhibit stronger photoabsorption properties due to its synergetic effect and significantly enhances the photocatalytic activity of the catalyst towards the dye degradation [41]. Another important factor responsible for efficient photocatalytic activity of the catalyst is the optimal band gap energy (2.8 Å) which significantly increases the electron hole pair generation. The proposed mechanism for photocatalytic degradation of MB and RhB in aqueous solution can be expressed as follows,

$$Zn^{II}Fe\ LDH\ +\ h\nu\ \rightarrow\ h^+\ +\ e^-$$

$$h^+\ +\ H_2O\ \rightarrow 2H^+\ +\ 2\dot{\ }OH$$

$$e^-\ +\ O_2\ \rightarrow\ O_2^{\dot{\ }-}$$

$$O_2^{\dot{\ }-}\ +\ H^+ \rightarrow HO_2^{\dot{\ }}$$

$$HO_2^{\dot{\ }}\ +\ HO_2^{\dot{\ }}\ \rightarrow\ H_2O_2\ +\ O_2$$

$$H_2O_2\ \rightarrow 2\dot{\ }OH$$

$$Dye\ +\ \dot{\ }OH\ \rightarrow Degraded\ Products$$

The degradation of MB takes place via the attack of $\dot{\ }OH$ radicals on $C–S^+=C$ functional group of the MB aromatic structure [50,51]. This induces the opening of the aromatic ring resulting in the formation of various smallest aliphatic compounds and finally mineralizing of the harmful organic dye pollutants into the harmless CO_2, H_2O, SO_4^{2-}, NH_4^+ and NO_3^- [47]. Similarly, degradation of rhodamine B takes place via the aromatic ring opening resulting in the formation of simplest non-toxic compounds. These smallest compounds then further break down to mineralized products such as CO_2 and H_2O [52].

Table 4B.2. Comparison of photocatalytic activity of ZnFe LDH with reported catalysts

Entry	Catalysts	Dye	Conc. (mg/L)	Vol. (mL)	Catalyst amount (mg)	Light source	Time (min)	Deg. (%)	Ref.
1	ZnFe LDH	MB	10	50	5	UV	180	99.9	[This work]
		RhB	10	50	10	UV	240	99.8	
2	WO₃-ZY	RhB	10	50	25	UV	140	86	[34]
3	Ni-catalyst assisted GaN nanowire	MB	10	50	–	UV	240	93	[53]
4	FeOOH-LDO	MB	3	50	175	Visible	180	95	[51]
5	Graphene-TiO₂ nanocomposite	RhB	5×10^{-5} mol/L	30	30	Solar	60	98	[54]
6	P-25 Degussa	MB	12×10^{-5} M	25	1.2 g/L	UV-LED	6h	100	[49]
7	Ni-Ti LDH	MB	0.3198	200	15	Visible	75	99.8	[55]
8	Hexagonal-MoO₃	MB	10	100	100	UV Visible	120	71.4 98.2	[56]

Table 4B.2 shows the comparison of photocatalytic activity of ZnFe LDH with various other reported catalysts in terms of percentage degradation and various reaction parameters. It is observed that ZnFe LDH exhibits efficient photocatalytic activity for degradation of MB and RhB from aqueous solution under UV light irradiation compared to the other photocatalysts.

4B.2   Reusability test of the photocatalyst

From industrial point of view, stability and reusability of a catalyst are two important factors. The stability of the catalyst has been determined from the use of the regenerated catalyst for photocatalytic degradation of MB and RhB over ZnFe LDH and is shown in Figure 4B.9. The catalyst was regenerated by centrifuging the used catalyst with water and finally with ethanol solution (five times) and then dried at 80 °C for overnight. The regenerated catalyst thus obtained was again subjected to another new cycle under similar experimental conditions keeping dye concentration and catalyst amount constant at pH 7. For both cases, it is observed that the photocatalytic efficiency of the catalyst is retained upto 90% even after five cycles.

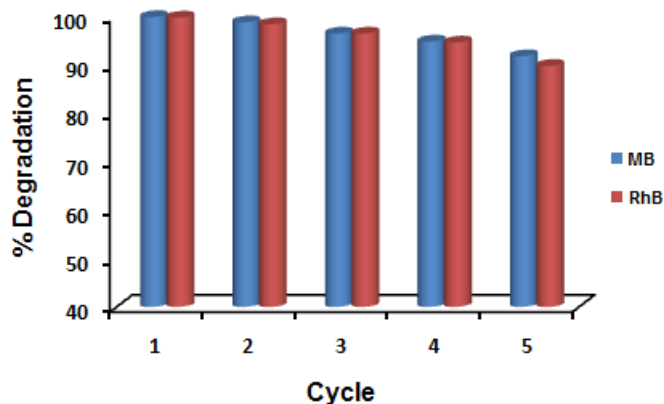**Figure 4B.9.** Recyclability test for photocatalytic degradation of MB and RhB over ZnFe LDH. (Conditions: $C_o = 10$ mg/L, $V_{solution} = 50$ mL, catalyst amount = 5 mg for MB and 10 mg for RhB, pH = 7).

To check the stability of the photocatalyst, XRD analysis was done after five reuses. Figure 4B.10 shows the XRD patterns of the reused and fresh catalyst. No

characteristic change in the XRD pattern is observed, demonstrating that the crystal structure of LDH is retained even after multiple reuses and thus, confirming the stable nature of the photocatalyst.
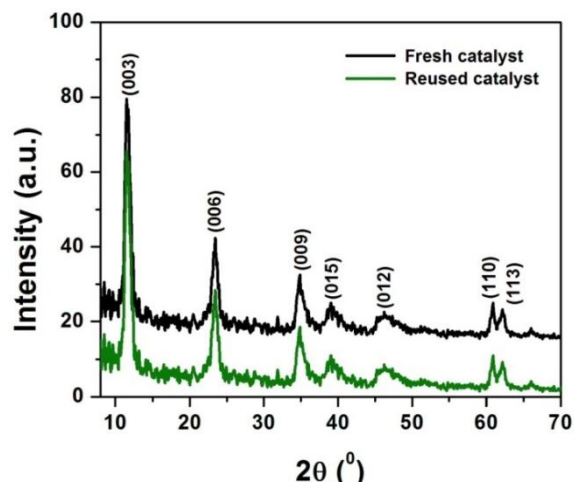
Figure 4B.10. XRD patterns of fresh and reused ZnFe LDH photocatalyst.

In summary, ZnFe LDH synthesized via a simple co-precipitation method has been employed as catalyst for photodegradation of MB and RhB in aqueous solution under UV and visible light irradiation. The photocatalyst shows excellent activity with 100% degradation towards the removal of MB and RhB in aqueous solution under UV light. Effects of various parameters such as irradiation time, catalyst amount, initial dye concentration and pH on photodegradation process have been studied in detail. The kinetic study shows that the photocatalytic degradation process followed first order kinetics for both cases. The recyclability of the catalyst have been studied and found to be active upto five cycles without any significant loss in the activity.

REFERENCES

[1] Seftel, E. M., Puscasu, M. C., Mertens, M., Cool, P., and Carja, G. Assemblies of nanoparticles of CeO_2–ZnTi-LDHs and their derived mixed oxides as novel photocatalytic systems for phenol degradation. *Applied Catalysis B: Environmental*, 150–151:157–166, 2014.

[2] Chowdhury, P., Moreira, J., Gomaa, H., and Ray, A. K. Visible-solar-light-driven photocatalytic degradation of phenol with dye-sensitized TiO_2: Parametric and kinetic study. *Industrial & Engineering Chemistry Research*, 51(12):4523−4532, 2012.

[3] Liu, D., Zheng, Z., Wang, C., Yin, Y., Liu, S., Yang, B., and Jiang, Z. CdTe quantum dots encapsulated ZnO nanorods for highly efficient photoelectrochemical degradation of phenols. *The Journal of Physical Chemistry C*, 117(50):26529−26537, 2013.

[4] Wu, Z.- L., Ondruschka, B., and Cravotto, G. Degradation of phenol under combined irradiation of microwaves and ultrasound. *Environmental Science & Technology*, 42(21):8083–8087, 2008.

[5] Zhou, S., Gu, C., Qian, Z., Xu, J., and Xia, C. The activity and selectivity of catalytic peroxide oxidation of chlorophenols over Cu–Al hydrotalcite/clay composite. *Journal of Colloid and Interface Science*, 357(2):447–452, 2011.

[6] Muhammad, S., Saputra, E., Sun, H., Ang, H. -M.,Tadé, M. O., and Wang, S. Heterogeneous catalytic oxidation of aqueous phenol on red mud-supported cobalt catalysts. *Industrial & Engineering Chemistry Research*, 51(47):15351−1535, 2012.

[7] Zhou, Y., Gu, X., Zhang, R., and Lu, J. Influences of various cyclodextrins on the photodegradation of phenol and bisphenol A under UV light. *Industrial & Engineering Chemistry Research*, 54(1):426−433, 2015.

[8] Grabowska, E., Reszczyńska, J., and Zaleska, A. Mechanism of phenol photodegradation in the presence of pure and modified-TiO_2: A review. *Water Research*, 46(17):5453–5471, 2012.

[9]   Puscasu, C. -M., Seftel, E. M., Mertens, M., Cool, P., and Carja, G. ZnTiLDH and the derived mixed oxides as mesoporous nanoarchitectonics with photocatalytic capabilities. *Journal of Inorganic and Organometallic Polymers and Materials*, 25(2):259–266, 2015.

[10]   Parida, K. M. and Pradhan, A. C. Fe/meso-Al_2O_3: An efficient photo-Fenton catalyst for the adsorptive degradation of phenol. *Industrial & Engineering Chemistry Research*, 49(18):8310–8318, 2010.

[11]   Koilraj, P. and Srinivasan, K. ZnAl layered double hydroxides as potential molybdate sorbents and valorize the exchanged sorbent for catalytic wet peroxide oxidation of phenol. *Industrial & Engineering Chemistry Research*, 52(22):7373−7381, 2013.

[12]   Al-Kandari, H., Abdullah, A. M., Mohamed, A. M., and Al-Kandari, S. Enhanced photocatalytic degradation of a phenolic compounds' mixture using a highly efficient TiO_2/ reduced graphene oxide nanocomposite. *Journal of Materials Science*, 51(18):8331–8345, 2016.

[13]   Saha, B., Das, S., Saikia, J., and Das, G. Preferential and enhanced adsorption of different dyes on iron oxide nanoparticles: A comparative study. *The Journal of Physical Chemistry C*, 115(16):8024–8033, 2011.

[14]   Pahalagedara, M. N., Samaraweera, M., Dharmarathna, S., Kou, C. -H., Pahalagedara, L. R., Gascón, J. A., and Suib, S. L. Removal of azo dyes: Intercalation into sonochemically synthesized NiAl layered double hydroxide. *The Journal of Physical Chemistry C*, 118(31):17801−17809, 2014.

[15]   Munagapati, V. S., and Kim, D. -S. Adsorption of anionic azo dye congo red from aqueous solution by cationic modified orange peel powder. *Journal of Molecular Liquids*, 220:540–548, 2016.

[16]   Zhu, S., Jiao, S., Liu, Z., Pang, G., and Feng, S. High adsorption capacity for dye removal by CuZn hydroxyl double salts. *Environmental Science: Nano*, 1:113–121, 2014.

[17]   Roy, A., Adhikari, B., and Majumder, S. B. Equilibrium, kinetic, and thermodynamic studies of azo dye adsorption from aqueous solution by chemically

modified lignocellulosic jute fiber. *Industrial & Engineering Chemistry Research*, 52(19):6502−6512, 2013.

[18]   Ai, L., Zhang, C., and Meng, L. Adsorption of methyl orange from aqueous solution on hydrothermal synthesized Mg-Al layered double hydroxide. *Journal of Chemical Engineering Data*, 56(11):4217–4225, 2011

[19]   He, S., Zhao, Y., Wei, M., Evans, D. G., and Duan, X. Fabrication of hierarchical layered double hydroxide framework on aluminium foam as a structured adsorbent for water treatment. *Industrial & Engineering Chemistry Research*, 51(1):285–291, 2012.

[20]   Mantilla, A., Jácome-Acatitla, G., Morales-Mendoza, G., Tzompantzi, F., and Gómez, R. Photoassisted degradation of 4-chlorophenol and *p*-cresol using MgAl hydrotalcites. *Industrial & Engineering Chemistry Research*, 50(5):2762–2767, 2011.

[21]   Malekshoar, G., Pal, K., He, Q., Yu, A., and Ray, A. K. Enhanced solar photocatalytic degradation of phenol with coupled graphene-based titanium dioxide and zinc oxide. *Industrial & Engineering Chemistry Research*, 53(49):18824−18832, 2014.

[22]   Chen, Q., Ji, F., Guo, Q., Guan, W., Yan, P., Pei, L., and Xu, X. Degradation of phenol by vis/Co-TiO$_2$/KHSO$_5$ hybrid Co/SR−photoprocess at neutral pH. *Industrial & Engineering Chemistry Research*, 52(35):12540−12549, 2013.

[23]   Pino, E. and Encinas, M. V. Photocatalytic degradation of chlorophenols on TiO$_2$−325mesh and TiO$_2$–P25. An extended kinetic study of photodegradation under competitive conditions. *Journal of Photochemistry and Photobiology A: Chemistry*, 242:20–27, 2012.

[24]   Tasbihi, M., Ngah, C. R., Aziz, N., Mansor, A., Abdullah, A. Z., Teong, L. K., and Mohamed, A. R. Lifetime and regeneration studies of various supported TiO$_2$ photocatalysts for the degradation of phenol under UV-C light in a batch reactor. *Industrial & Engineering Chemistry Research*, 46(26):9006−9014, 2007.

[25]   Wang, M., Han, J., Hu, Y., Guo, R., and Yin, Y. Carbon-incorporated NiO/TiO$_2$ mesoporous shells with p–n heterojunctions for efficient visible light photocatalysis. *ACS Applied Materials & Interfaces*, 8(43):29511−29521, 2016.

[26]   Méndez-Medrano, M. G., Kowalska, E., Lehoux, A., Herissan, A., Ohtani, B., Rau, S., Colbeau-Justin, C., Rodríguez-López, J. L., and Remita, H. Surface modification of TiO_2 with Au nanoclusters for efficient water treatment and hydrogen generation under visible light. *The Journal of Physical Chemistry C*, 120(43):25010−25022, 2016.

[27]   Aleksandrzak, M., Adamski, P., Kukułka, W., Zielinska, B., and Mijowska, E. Effect of graphene thickness on photocatalytic activity of TiO_2-graphene nanocomposites. *Applied Surface Science*, 331:193–199, 2015.

[28]   Lan, M., Fan, G., Yang, L., and Li, F. Significantly enhanced visible-light-induced photocatalytic performance of hybrid Zn−Cr layered double hydroxide/graphene nanocomposite and the mechanism study. *Industrial & Engineering Chemistry Research*, 53(33):12943−12952, 2014.

[29]   Zhou, Y., Hu, W., Yu, J., and Jiao, F. Effective photocatalytic degradation of methylene blue by Cu_2O/MgAl layered double hydroxides. *Reaction Kinetics, Mechanisms and Catalysis*, 115(2):581–596, 2015.

[30]   Zou, Y., Wang, X., Wu, F., Yu, S., Hu, Y., Song, W., Liu, Y., Wang, H., Hayat, T., and Wang, X. Controllable synthesis of Ca-Mg-Al layered double hydroxides and calcined layered double oxides for the efficient removal of U(VI) from wastewater solutions. *ACS Sustainable Chemistry & Engineering*, 5(1):1173−1185, 2017.

[31]   Parida, K., Mohapatra, L., and Baliarsingh, N. Effect of Co^{2+} substitution in the framework of carbonate intercalated Cu/Cr LDH on structural, electronic, optical, and photocatalytic properties. *The Journal of Physical Chemistry C*, 116(42):22417−22424, 2012.

[32]   Liang, H., Li, L., Meng, F., Dang, L., Zhuo, J., Forticaux, A., Wang, Z., and Jin, S. Porous two-dimensional nanosheets converted from layered double hydroxides and their applications in electrocatalytic water splitting. *Chemistry of Materials*, 27(16):5702−5711, 2015.

[33]   Parida, K. M. and Mohapatra, L. Carbonate intercalated Zn/Fe layered double hydroxide: A novel photocatalyst for the enhanced photo degradation of azo dyes. *Chemical Engineering Journal*, 179:131–139, 2012.

[34] Jothivenkatachalam, K., Prabhu, S., Nithya, A., and Jeganathan, K. Facile synthesis of WO_3 with reduced particle size on zeolite and enhanced photocatalytic activity. *RSC Advances*, 4:21221–21229, 2014.

[35] Zaghouane-Boudiaf, H., Boutahala, M., and Arab, L. Removal of methyl orange from aqueous solution by uncalcined and calcined MgNiAl layered double hydroxides (LDHs). *Chemical Engineering Journal*, 187:142–149, 2012.

[36] Zhang, M., Yao, Q., Lu, C., Li, Z., and Wang, W. Layered double hydroxide−carbon dot composite: High- performance adsorbent for removal of anionic organic dye. *ACS Applied Materials & Interfaces*, 6(22):20225−20233, 2014.

[37] Tzompantzi, F., Mantilla, A., Bañuelos, F., Fernández, J. L., and Gómez, R. Improved photocatalytic degradation of phenolic compounds with ZnAl mixed oxides obtained from LDH materials. *Topics in Catalysis*, 54(1):257–263, 2011.

[38] Valente, J. S., Tzompantzi, F., and Prince, J. Highly efficient photocatalytic elimination of phenol and chlorinated phenols by CeO_2/MgAl layered double hydroxides. *Applied Catalysis B: Environmental*, 102(1–2):276–285, 2011.

[39] Dixit, A., Mungray, A. K., and Chakraborty, M. Photochemical oxidation of phenol and chlorophenol by $UV/H_2O_2/TiO_2$ process : A kinetic study. *International Journal of Chemical Engineering and Applications*, 1(3):247–250, 2010.

[40] Ahmed, S., Rasul, M. G., Brown, R., and Hashib, M. A. Influence of parameters on the heterogeneous photocatalytic degradation of pesticides and phenolic contaminants in wastewater: A short review. *Journal of Environmental Management*, 92(3):311–330, 2011.

[41] Gaya, U. I. and Abdullah, A. H. Heterogeneous photocatalytic degradation of organic contaminants over titanium dioxide: A review of fundamentals, progress and problems. *Journal of Photochemistry and Photobiology C: Photochemistry. Reviews*, 9(1):1–12, 2008.

[42] Parida, K., Satpathy, M., and Mohapatra, L. Incorporation of Fe^{3+} into Mg/Al layered double hydroxide framework: Effects on textural properties and

photocatalytic activity for H$_2$ generation. *Journal of Material Chemistry*, 22(15):7350–7357, 2012.

[43] Baliarsingh, N., Parida, K. M., and Pradhan, G. C. Effects of Co, Ni, Cu, and Zn on photophysical and photocatalytic properties of carbonate intercalated M^{II}/Cr LDHs for enhanced photodegradation of methyl orange. *Industrial & Engineering Chemistry Research*, 53(10):3834–3841, 2014.

[44] Cao, F., Shi, W., Zhao, L., Song, S., Yang, J., Lei, Y., and Zhan, H. Hydrothermal synthesis and high photocatalytic activity of 3D wurtzite ZnSe hierarchical nanostructures. *The Journal of Physical Chemistry C*, 112(44):17095–17101, 2008.

[45] Guo, Z., Ma, R., and Li, G. Degradation of phenol by nanomaterial TiO$_2$ in wastewater. *Chemical Engineering Journal*, 119(1):55–59, 2006.

[46] Liu, L., Liu, H., Zhao, Y. - P., Wang, Y.,Duan, Y., Gao, G., Ge, M., and Chen, W. Directed synthesis of hierarchical nanostructured TiO$_2$ catalysts and their morphology-dependent photocatalysis for phenol degradation. *Environmental Science & Technology*, 42(7):2342–2348, 2008.

[47] Darabdhara, G., Boruah, P. K., Borthakur, P., Hussain, N., Das, M. R., Ahamad, T., Alshehri, S. M., Malgras, V., Wu, K. C. -W., and Yamauchi, Y. Reduced graphene oxide nanosheets decorated with Au–Pd bimetallic alloy nanoparticles towards efficient photocatalytic degradation of phenolic compounds in water. *Nanoscale*, 8(15):8276–8287, 2016.

[48] Zhurko, G. and Zhurko, D. Chemcraft, Version 1.7 (build 365), 2013.

[49] Tayade, R. J., Natarajan, T. S., and Bajaj, H. C. Photocatalytic degradation of methylene blue dye using ultraviolet light emitting diodes. *Industrial & Engineering Chemistry Research*, 48(23):10262–10267, 2009.

[50] Houas, A., Lachheb, H., Ksibi, M., Elaloui, E., Guillard, C., and Herrmann, J. -M. Photocatalytic degradation pathway of methylene blue in water. *Applied Catalysis B: Environmental*, 31(2):145–157, 2001.

[51] Xia, S., Zhang, L., Pan, G., Qian, P., and Ni, Z. Photocatalytic degradation of methylene blue with a nanocomposite system: Synthesis, photocatalysis and

degradation pathways. *Physical Chemistry Chemical Physics*, 17:5345–5351, 2015.

[52]   Baldev, E., MubarakAli, D., Ilavarasi, A., Pandiara, D., Ishack, K. A. S. S., and Thajuddin, N. Degradation of synthetic dye, rhodamine B to environmentally non-toxic products using microalgae. *Colloids and Surfaces B: Biointerfaces*, 105:207–214, 2013.

[53]   Purushothaman, V., Prabhu, S., Jothivenkatachalam, K., Parthiban, S., Kwon, J. Y., and Jeganathan, K. Photocatalytic dye degradation properties of wafer level GaN nanowires by catalytic and self-catalytic approach using chemical vapor deposition. *RSC Advances*, 4:25569–25575, 2014.

[54]   Posa, V. R., Annavaram, V., Koduru, J. R., Bobbala, P., and Somala, A. R. Preparation of graphene–TiO_2 nanocomposite and photocatalytic degradation of rhodamine-B under solar light irradiation. *Journal of Experimental Nanoscience*, 11(9):722-736, 2016.

[55]   Chowdhury, P. R. and Bhattacharyya, K. G. Ni/Ti layered double hydroxide: Synthesis, characterization and application as a photocatalyst for visible light degradation of aqueous methylene blue. *Dalton Transactions*, 44:6809–6824, 2015.

[56]   Chithambararaj, A., Sanjini, N. S., Bose, A. C., and Velmathi, S. Flower-like hierarchical h-MoO_3: New findings of efficient visible light driven nano photocatalyst for methylene blue degradation. *Catalysis Science & Technology*, 3:1405–1414, 2013.